NASA Technical Paper 1159

Combustion of Hydrogen in a Two-Dimensional Duct With Step Fuel Injectors

James M. Eggers, Patricia G. Reagon,
and Paul B. Gooderum

MAY 1978

NASA

NASA Technical Paper 1159

Combustion of Hydrogen in a Two-Dimensional Duct With Step Fuel Injectors

James M. Eggers, Patricia G. Reagon, and Paul B. Gooderum
Langley Research Center
Hampton, Virginia

SUMMARY

An investigation of the combustion of hydrogen perpendicularly injected from step fuel injectors into a Mach 2.72, 2100 K vitiated test gas was conducted. The model simulated the flow between the center and side struts of an integrated scramjet module at Mach 7 flight and an altitude of 29 km. Parametric variation included equivalence ratio, fuel dynamic pressure ratio, and area distribution of the model. The overall area ratio of the model was held constant at 2.87. Data acquired were wall static-pressure distributions, heat-transfer distributions, total heat transfer to the model, and pitot and gas concentration measurements in the model exit. The data analysis indicated that no measurable improvement in mixing or combustion efficiency was obtained by varying the fuel dynamic pressure ratio from 0.79 to 2.45. Computations indicated approximately 80 percent of the fuel was mixed so that it could react; however, only approximately 50 percent of the mixed fuel actually reacted in two test configurations, and 74 percent in later tests where less area expansion of the flow occurred. A possible reason for the poor reaction (50 percent) is believed to be associated with adverse pressure interactions of the upstream injection process upon the downstream injection region. One-dimensional analysis also suggests that flow expansion tended to suppress the rate of reaction. The inability of the sample probe to quench the reaction in the gas samples prevented determination of local combustion efficiencies. Recommendations for future work are also discussed.

INTRODUCTION

Recent hypersonic vehicle and engine configuration studies have led to the hydrogen-fueled airframe-integrated scramjet concept as described in reference 1. In this concept, the forebody of the flight vehicle serves as a compression surface for the inlets of a number of engine modules as illustrated in figure 1. The remainder of the inlet compression is accomplished by use of swept struts which span the combustor inlet interface. The swept struts provide a potentially convenient means of supplying and distributing the hydrogen fuel through both normal and parallel modes of fuel injection. The potential for good performance over a flight Mach number range is provided by scheduling different proportions of fuel between the normal and parallel injector modes. In order to achieve good performance, for example, high combustion efficiency and low cooling losses, the location, size, and distribution of fuel injection orifices must be optimized; that is, the fuel must be distributed, mixed, and reacted in as short a physical distance as possible with a minimum of losses.

Recent work related to supersonic combustor design is reported in references 2 to 11. These references include both nonreacting and reacting flow studies with parallel injection (refs. 2 and 3), cross-stream injection (refs. 4 and 5), exploratory scramjet and combustor development (refs. 6 to 8), and injection from struts (refs. 9 and 10). The results of these studies have provided a data base identifying problem areas such as ignition behavior,

finite reaction rates, unmixedness, and the need to improve turbulent transport models and three-dimensional flow computational capability in order to better model the flows. However, even for basic simple geometry reacting flows, the current analytical tools cannot be applied with confidence due largely to the complexity of the flow field and associated uncertainties in the turbulent mixing models. Therefore, scramjet combustor design relies on experimental correlations and requires experimental evaluation for proof of performance.

This report documents a study of normal injection and combustion of hydrogen in a two-dimensional duct with step changes in area. (Some preliminary results of this study are reported in ref. 12.) The duct geometry simulates the flow between the center and side strut in an integrated scramjet module previously discussed. Nominal duct inlet conditions for the test were Mach 2.72, a total temperature of 2100 K, and a stagnation pressure of 2.9 MN/m^2. Duct inlet static pressures were approximately 0.11 MN/m^2. (Limited data were acquired at a lower total temperature of 1670 K.) The nominal temperature conditions correspond to Mach 7 flight enthalpy at an altitude of 29 km. The test gas was supplied by a hydrogen-fueled, oxygen-replenished combustion heater. The duct has provision for fuel injection at two longitudinal locations, one on the top and the other on the bottom of the duct. Parameters which were varied are the ratio of fuel dynamic pressure to free-stream dynamic pressure, equivalence ratio, the number and size of the circular fuel injectors orifices, the area distribution of the model, and the shape of the fuel injection steps. The overall area ratio of the model was constant at a value of 2.87.

Data acquired were wall static pressures, local heat transfer, pitot and gas sample measurements, and total heat transfer to the model. The wall static pressures were used in a one-dimensional analysis to infer the combustion efficiency distribution and overall combustion efficiency of the model.

SYMBOLS

A	area
A_b	refers to fuel injection block (fig. 4(b))
A_t	refers to fuel injection block (fig. 4(a))
A_x	refers to test configuration with area distribution changed from that of basic Q_3 and Q_1 configurations (fig. 3)
B_b	refers to fuel injection block (fig. 4(b))
B_t	refers to fuel injection block (fig. 4(a))
C_b	refers to fuel injection block (fig. 4(d))
C_D	orifice discharge coefficient
C_f	friction coefficient

C_t refers to fuel injection block (fig. 4(c))

E_r reaction efficiency, a measure of how far chemical reaction has
             proceeded toward completion, η_c/η_m

F   thrust function, $(p + \rho V^2)A$

H_t total enthalpy

h   model exit height, 11.2 cm (fig. 3)

M   Mach number

p   static pressure

P_t stagnation pressure

Q   local heat transfer to model

$\bar{Q}$ total heat transfer to model

Q_1 refers to test configuration with fuel injectors sized for injection
             at a ratio of fuel dynamic pressure to free-stream dynamic pressure
             of 1 at $\phi = 1$ (fig. 3)

Q_3 refers to test configuration with fuel injectors sized for injection
             at a ratio of fuel dynamic pressure to free-stream dynamic pressure
             of 3 at $\phi = 1$ (fig. 3)

T   static temperature

T_t stagnation temperature

V   velocity

W   mass flow through model including hydrogen fuel

x   longitudinal coordinate measured from model entrance (fig. 3)

y   vertical coordinate (fig. 3)

η_c combustion efficiency, fraction of injected hydrogen fuel
             which reacted

η_m mixing efficiency, fraction of injected hydrogen fuel mixed so
             that it could react

ρ density

ϕ equivalence ratio, ratio of fuel mass fraction to fuel mass fraction
             required to react all oxygen in test gas, $\phi = \phi_t + \phi_b$

3

Subscripts:

b   bottom fuel injection

e   model exit

h   combustion heater

t   top fuel injection

1   model entrance

APPARATUS

Model

The relation of the two-dimensional step injection model to the integrated scramjet geometry is shown in figure 2. The model simulates the flow between the center and side struts of the inlet of an engine module. The combustor model top wall corresponds to the streamline downstream of the trailing edge of the center strut and the bottom wall corresponds approximately to a streamline downstream of the trailing edge of a side strut. The model length to height ratio (height of model is equivalent to strut gap in engine) is approximately 20 as compared with a value of 48 for the current scramjet module design concept. Nonuniformity of inlet flow, shock structure, boundary layer, strut sweep, and the ratio of model inlet height (strut gap) to model engine length were not simulated. Total enthalpy, Mach number, and static-pressure levels were adequately simulated to provide meaningful results.

The geometry of the model is shown in figure 3. The model has an overall length of 78.7 cm and a constant width of 17.0 cm. The model entrance height is 3.89 cm and its exit height is 11.2 cm; thus, the overall area ratio is 2.87. A 20-percent area increase occurs through the fuel injector region; hydrogen fuel is injected perpendicular to the main flow through circular orifices from the top and bottom walls immediately downstream of the steps. The small downstream steps in the top and bottom walls simulate the blunt base region at the rear end of the engine module struts. The steps ahead of the fuel injectors are intended to isolate the pressure rise due to combustion and injection interactions from the upstream flow field, and thus prevent upstream separation. Injection was intended to occur close enough to the injector block steps to be within the recirculation region, and thus promote ignition, penetration, and mixing. The model was basically water cooled; the fuel injector blocks received some fuel cooling, and a short extension block and extension side walls at the end of the duct relied on heat sink cooling.

Three configurations of the model were tested by using combinations of the fuel injection blocks shown in figure 4. Blocks identified with particular configurations are listed in figure 3. Configuration Q_3 employed top injector block A_t (fig. 4(a)) and lower injector block A_b (fig. 4(b)). The injector orifices for configuration Q_3 were sized for fuel injection at a ratio of fuel

4

dynamic pressure to free-stream dynamic pressure of 3 (thus Q_3), equal injections from each block, and an overall equivalence ratio of unity. The four 0.295-cm-diameter orifices in the top block and three 0.343-cm-diameter orifices in the bottom block were longitudinally displaced by 5.08 cm and laterally interdigitated as shown in figures 4(a) and 4(b). Conceptually, each injection orifice would supply fuel to a rectangular region equal to one-half the duct height and a width equal to the spacing between the orifices.

Configuration Q_1 differed from configuration Q_3 only by the size of the injection orifices. The orifices in the top block were enlarged to 0.516-cm diameter and the bottom injector orifices to 0.594-cm diameter (figs. 4(a) and 4(b)) to provide injection at a ratio of fuel dynamic pressure to free-stream dynamic pressure of 1 (thus Q_1). Tests with configurations Q_3 and Q_1 were intended to determine the effect of variation in the ratio of fuel dynamic pressure to free-stream dynamic pressure on performance.

Configuration A_x evolved from the results of the Q_3 and Q_1 configuration tests when poorer combustion efficiency than anticipated was indicated. The injector blocks for the A_x configuration are shown in figures 4(c) and 4(d). The step in the top injector was replaced with a ramped surface and nine 0.159-cm-diameter orifices were interspaced between the larger orifices The bottom injector block was modified by replacing the three large orifices by six smaller 0.277-cm-diameter orifices. In addition, the area distribution of the model was modified by reducing the wall angles by one-half immediately downstream of the injection region (fig. 3) but maintaining the same overall area ratio of the model. A photograph of the model as installed for testing is shown in figure 5.

Facility

Hot test gas was supplied to the model by a hydrogen-fueled oxygen-replenished combustion heater. The design and performance of the heater are documented in references 13 to 15. Nominal test-gas conditions for the current tests correspond to an enthalpy level representative of Mach 7 flight at an altitude of 29 km, a model entrance Mach number of 2.72, a total temperature of 2100 K (static temperature of 1060 K), and a total pressure of 2.9 MN/m^2. Model inlet static pressures were approximately 0.11 MN/m^2. (A limited amount of wall static and heat-transfer data were acquired at a reduced total temperature of 1670 K.) For the nominal test condition, the test-gas flow rate was 3.96 kg/sec and contained approximately 21-percent oxygen, 32-percent water, and 46-percent nitrogen by volume.

Test Procedure and Instrumentation

Tests were conducted by establishing preset flow rates to the combustion heater. Approximately 2 seconds later, preset fuel flow rates were established to the injectors. About 3 seconds were required for the heater to reach steady state and a similar but overlapping time period for the fuel flow to be estab-

lished. Typical test runs were 15 seconds in duration with an available data acquisition period of about 10 to 12 seconds.

Two oscillographs, an FM tape system and a digital data system, were simultaneously employed to record the data. The data system provided post run display of the parameters to define the test-gas and hydrogen fuel injection conditions.

Pressures and temperatures necessary to define the heater test gas, model top and bottom wall static-pressure distributions, hydrogen fuel flow rates to each of the top and bottom fuel injector blocks, and coolant flow rates and temperatures to determine overall and local heat transfer to the model were measured. Typical wall instrumentation is shown in figure 6; each shaded region consisted of either a knuckle joint or a block insert which had independent cooling circuits from the model proper for deducing local heat transfer.

A nine probe survey rake was used to measure pitot pressures and collect gas samples. Complete mapping of the model exit required multiple tests, as the test time prohibited multiple location gas sample collection and thus some variation in heater and injection conditions. Five tests with probe measurements at five locations (45 data points) were used to map the exit flow for the Q_3 and Q_1 configurations. One less survey (36 data points) was employed to map the model exit for the A_x configuration. Lateral and vertical probe spacing was 1.9 cm.

Gas samples were collected in 75-cc sample cylinders by use of a nine probe pitot gas-sampling rake. (See fig. 5.) Collection procedure consisted of purging the preevacuated cylinders with the gas sample and then collecting the sample to above atmospheric pressure. The samples were analyzed after the run by use of a gas chromatograph to determine helium (tracer gas contained in the oxygen supply to the heater), hydrogen, oxygen, and nitrogen content. The water in the gas sample, due to both the combustion heater products and the combustion hydrogen in the model was not analyzed but was computed from knowledge of the oxygen and airflow rates to the heater and the helium tracer gas in the oxygen. Similar procedures were used and a more complete description of the entire gas collection and analysis procedure may be found in references 4, 5, and 14.

Accuracy

Combustion heater.- Based on an estimate of ±2-percent uncertainty in the individual metered heater flow rates of hydrogen, oxygen, and air, it is estimated the average heater total temperature is known within ±2 percent. (Heater data reported in ref. 15 indicate temperature nonuniformity on the order of ±3.5 percent due to fuel and air distributions.) Since the heater stagnation pressure is read by three independent and calibrated transducers, the heater stagnation pressure is believed to be known to within ±1 percent. Using these uncertainties in pressure and temperature, the heater flow rate is estimated to be accurate to within ±3 percent. Repeatability is an additional area of concern where experimental results are compared from a series of tests. In the current tests, the oxygen composition ranged from 19.9 to 22.7 percent on a

6

test-to-test basis as compared with a target value of 21 percent. No effect of this variation was detectable in the data.

Hydrogen fuel flow rates.- Hydrogen fuel flow rates were measured by sharp edge orifice meters. Estimated accuracies and calculated discharge coefficients are given in the following table for equivalence ratios near 0.9:

Configuration	Top injectors			Bottom injectors		
	Block	Flow rate accuracy, percent	C_D	Block	Flow rate accuracy, percent	C_D
Q_3	A_t	±2	0.83	A_b	±4	0.86
Q_1	B_t	±2	.59	B	±2	.68
A_x	C_t	±2	.61	C_b	±4	.86

The accuracies of the bottom injector flow rates for the Q_3 and A_x configurations were affected by a faulty check valve which induced occasional spurious signals in the orifice meter differential pressure measurement at high injection pressures; thus, the quoted accuracies are lower.

For equivalence ratios near 0.5 (configuration Q_1), the injectors were not choked and discharge coefficients could not be computed. For configurations Q_3 and A_x, the injectors remained choked and the C_D values were essentially identical to the tabulated values.

Gas analysis.- The accuracy of the gas analysis was checked by summing the volume fractions of the constituents. The summation was typically within 1 percent of unity for about 95 percent of the samples analyzed; the remaining samples were generally within ±2 percent of unity. The uncertainty of the analysis is insignificant relative to the uncertainty in sample collection from the high temperature reacting flow, and approximate data reduction techniques necessitated by the fact that the probe did not quench the reaction.

Analysis of the pitot pressure and gas sample data indicated that the probe measurements failed to account for a significant fraction, up to 26 percent, of the total mass flow through the model. Further sensitivity analysis indicated that the only measured parameter which could explain the discrepancy was the gas sample measurement, specifically the quenching ability of the probe. It was evident from this analysis that the flow at the model exit was far from completely reacted and that the probe essentially completed the reaction.

DATA ANALYSIS METHODS

Two computer programs were used to process the data; a one-dimensional program to process the wall data and an integral program to process the probe survey data. Theoretically, the combustion efficiency of the test configuration could be derived from the wall static-pressure measurements by use of the one-dimensional program and compared with the value derived from the probe data by use of the integral program. However, as the model exit flow was incompletely reacted and the probe failed to quench the reaction, comparisons of combustor efficiency derived from the two techniques were not possible. The erroneous probe data also necessitated corrections to be applied to the composition and pitot pressure data. The programs and corrections are discussed in the following paragraphs.

One-Dimensional Analysis Program

The one-dimensional analysis program, COMBAN, is a real-gas equilibrium chemistry program which used the measured wall static pressures to infer combustion efficiency and heat-transfer distributions for the model. Principal inputs are the facility nominal test conditions, the model area distribution, the wetted perimeter distribution, the model wall temperature, the friction coefficient, and the wall static-pressure distribution. At each computational step in the program, enough fuel is allowed to react to match the measured static pressure. (Similar versions of this program have been used. See refs. 4, 5, 10, and 11.) Stagnation pressure losses due to shocks are neglected; therefore, the technique is limited to flow fields where total-pressure losses due to heat addition dominate, which is assumed to be the case for the current experiment. Reynolds analogy is employed to compute the heat transfer. In regions of adverse pressure gradient, a multiplier of 1.6 (based on the combustor data analysis of ref. 16) was employed to increase the heat transfer. (Neglect of this factor typically reduces the heat transfer about 7 percent for the current test data.) A constant value of friction coefficient was selected to force agreement between the computed and measured total heat transfer to the model. The computed values of combustion efficiency are sensitive to the specified pressure distribution. Sensitivity studies here and in reference 4 indicate that the combustion efficiency uncertainty is on the order of ±12 to 15 percent.

The inverse of this computation was also employed to compute the pressure distribution for zero fuel injection and for estimating the pressure distribution for a given distribution of combustion derived from cold mixing studies. (Similar computations are reported in ref. 4.) In the latter computation the cold mixing efficiency is assumed to be equal to the combustion efficiency.

Integral Program

The integral program, COPEIN, uses the discrete corrected pitot pressure and fuel concentration data and a constant value of reaction efficiency from the one-dimensional analysis and generates a continuous distribution of measured properties over the model exit plane by use of a cubic spline surface

routine. (A reaction efficiency distribution would have been specified from the gas samples if the reaction had been quenched by the probe.) From the continuous distribution, a 20 × 20 grid system is established and values of the pitot pressure and fuel concentration are determined at each grid point. From these values, knowledge of the test-gas composition of the facility, and heat loss to the facility and model, all other flow properties are computed on the grid.

Specifically, the total enthalpy is known at each point from the fuel concentration, test-gas composition, and heat losses. The heat losses are subtracted uniformly from the entire flow. (Sensitivity studies indicated that neglect of the combustor heat loss resulted in only a 2-percent change in mass flow.) As instream temperature measurements are not made, an iterative scheme was employed. A static temperature was assumed and gas properties were determined by using the composition, the reaction efficiency from COMBAN, and an assumption of uniform static pressure equal to the data value. The local Mach number was computed and used with the Rayleigh pitot formula to compute pitot pressures. The procedure was repeated until the computed and measured pitot pressures were in agreement. Gas properties were computed assuming no dissociation, but real-gas specific heats were employed.

From the computed properties at the grid points, integration over the exit area is performed to determine mass flows, mixing efficiency, reaction efficiency, total enthalpy, or any other desired parameter. In addition, the program contains the capability to generate contours of any desired parameter, for example, Mach number, equivalence ratio, etc.

Data Corrections

Fuel composition corrections.- As a standard procedure, the fuel concentration was uniformly scaled to force agreement between the value of equivalence ratio derived from the integral program and the value derived from the measured fuel and test-gas flow rates. This processing corrected for probe biasing effects, which occur even in nonreacting turbulent flow, and resulted in data which had the correct ratio of fuel to test gas. After this correction, the magnitudes of the hydrogen and test-gas flow rates were in error (low) because of the inability of the probe data to reflect the state of the hydrogen fuel, for example, reacted or unreacted. Therefore, the value of reaction efficiency derived from the one-dimensional analysis program was uniformly applied to the composition data. Note that the imposition of the reaction efficiency had only a second-order effect on the value of φ and thus did not require an iterative computation. The resultant mass flows computed with the integral program were in good agreement, within 11 percent of the metered values, once the pitot correction discussed in the following paragraph was incorporated into the computation.

Pitot pressure correction.- In a reacting flow, some degree of reaction can occur between the shock in front of the probe and the probe orifice reaction. This may cause the sensed pitot pressure to be lower than the pitot pressure if no reaction occurred in the probe flow field. A pitot pressure correction was computed by assuming the flow reacted completely immediately

behind the probe shock in a constant pressure process and then decelerated isentropically to stagnation conditions at the probe orifice. This assumption produces the greatest change in sensed pitot pressure for a given amount of heat release in the probe flow field. Calculated pitot pressure increases were in the range of 3 to 12 percent and resulted in an increase in calculated total mass flow in the range of 3 to 6 percent. All data were corrected as discussed and analyzed by use of the previously described computer programs.

RESULTS AND DISCUSSION

Test conditions corresponding to all data are presented in table I and cross referenced in the figures. Both the top and bottom injector and the overall equivalence ratio are given in the table. For discussion purposes, the equivalence ratios will be referred to as $\phi = 0$, $\phi = 0.5$, and $\phi = 0.9$, corresponding to no fuel injection, measured ϕ from 0.42 to 0.48, and measured ϕ from 0.87 to 1.02.

Wall Static-Pressure Distributions

$\phi = 0$.- The nondimensional wall static-pressure distribution is presented in figure 7 for the Q_3 and Q_1 configurations and in figure 8 for the A_x configuration. The ambient pressure to which the model exhausted is 0.9 in terms of p/p_1 for all data presented. Noteworthy features of the Q_3 and Q_1 configuration data (fig. 7) are a shock-induced pressure rise on the top wall near x of 25 cm, and separation of the flow from the top wall at x near 55 cm and from the bottom wall near 68 cm. The A_x configuration data (fig. 8) reflect both the change in the area distribution of the model and the change in the top injector block from a step to a ramped surface. The area change has resulted in higher pressures in the region from about 5 to 40 cm and the injector change has eliminated the low base pressure on the top injector at x = 4.4 cm.

$\phi = 0.5$.- Wall static-pressure distributions for $\phi = 0.5$ are presented in figures 9, 10, and 11 for configurations Q_3, Q_1, and A_x, respectively. Comparison with figures 7 and 8 for the corresponding configuration for $\phi = 0$ indicates a general increase in pressure with injection and is an indication of reaction. The pressure distribution for the A_x configuration is higher than that for the Q_3 and Q_1 configurations; however, as the area distribution differs, whether the higher pressure is indicative of more reaction is not apparent without further analysis. In the region immediately downstream of the injectors, it is impossible to separate local pressure rises associated with injection disturbances from those due to combustion.

$\phi = 0.9$.- Wall static-pressure distributions for $\phi = 0.9$ are presented in figures 12, 13, and 14 for configurations Q_3, Q_1, and A_x, respectively. The data indicate further pressure rise above that for $\phi = 0.5$ and thus further reaction. (Compare figs. 12, 13, and 14 with figs. 9, 10, and 11, respectively.) Based on the nearly identical static-pressure distributions for the Q_3 and Q_1 configurations, equivalent reaction distributions would be anticipated. This observation was substantiated by one-dimensional analysis of the data reported later in this paper.

The wall static-pressure distribution for the A_x configuration and a reduced stagnation temperature of 1670 K, as opposed to the nominal value of 2100 K, is presented in figure 15. Note the scale change relative to figures 7 to 14. The pressure increase due to injection and reaction is significantly higher for this test condition and caused flow separation to occur forward into the heater nozzle. Apparently, the step size was too small to provide isolation of the downstream pressure rise at these test conditions.

Modified Injector Tests

Upon completion of the Q_3 and Q_1 configuration tests, it was realized that anticipated combustion efficiencies, as evidenced by static-pressure levels in the model, were not achieved. Several injector modifications were employed with the basic idea of establishing faster and more rapid ignition in the hope that once the higher rate of heat release was established, it would be self-sustaining. Principal measurements to evaluate those tests were wall static pressures. Specific injector block modifications included increasing fuel concentration in the base region of the injector block step by the addition of extra holes (fig. 4(c)), ramping the injector block to eliminate the fuel-rich region established by the additional injection holes (fig. 4(c)), and injecting upstream of the step on the lower injection block through six orifices 0.28 cm in diameter. The latter is similar to injection block C_b (fig. 4(d)) with the orifices located upstream of the step but inclined 30° toward the upstream direction. All these modifications were unproductive as no indication was found of improved performance based on wall pressures, limited gas sample measurements, and heat-transfer data; therefore, no data are presented.

Wall Heat-Transfer Distributions

Wall heat-transfer distributions for $\phi = 0$ and $\phi = 0.9$ are presented in figures 16, 17, and 18 for the Q_3, Q_1, and A_x configurations, respectively. Distributions for nominal $\phi = 0.5$ are not presented because of the data scatter associated with measuring small temperature differences. Differences in heat transfer between $\phi = 0$ and $\phi = 0.9$ are attributed to reaction. Based on this observation, comparison of figures 16 and 17 suggests very similar reactions for the Q_3 and Q_1 configurations and a higher reaction for the A_x configuration (fig. 18).

Model Exit Contours

The equivalence ratio contours derived from the probe data are presented in figures 19 to 21, the Mach number contours in figures 22 to 24, and total temperature contours in figures 25 to 27. All contour data correspond to $\phi = 0.9$ as no probe data were taken for $\phi = 0.5$. The lateral location of the fuel injectors is indicated in the figures.

The equivalence ratio contours contain all the injected fuel, both reacted and unreacted. Particular features of the Q_3 and Q_1 configuration contours (figs. 19 and 20) are fuel-rich regions in line with the fuel injectors and

significantly better penetration of the top injectors as opposed to the bottom; for example, compare the distance between the wall and the region of maximum equivalence ratio. The poor penetration from the bottom injectors results in higher peak equivalence ratios than the relative number of injection orifices would lead one to expect. The poor penetration is believed to be due to imposed pressures on the bottom injection region arising from the top upstream injection and is discussed later. Mixing efficiencies were computed to be 83 percent and 79 percent for the Q_3 and Q_1 configurations, respectively.

In contrast to the fuel-rich regions in line with the injectors for the Q_3 and Q_1 configurations, the contours for the A_x configuration (fig. 21) have become stratified with nearly uniform fuel-rich regions adjacent to each wall and a fuel-lean region which spans the center region of the model exit. The flow stratification suggests the use of too many injectors. The mixing efficiency was computed to be 79 percent (essentially identical for all configurations).

The principal features of the Mach number contours (figs. 22 to 24) are lower Mach numbers in the fuel-rich regions. This is due both to the combustion process causing a stagnation pressure decrease, hence lower Mach number, and to losses associated with the injection process.

The total temperature contours for the Q_3 and Q_1 configurations (figs. 25 and 26) show lower total temperatures in the fuel-rich regions associated with the lower injectors; however, the range of total temperature values is fairly narrow and not nearly as well defined as the equivalence ratio and Mach number contours. In comparison with the Q_3 and Q_1 configuration profiles, the peak and average temperatures of the A_x configuration profiles (fig. 27) are significantly higher. This result is consistent with previous higher combustion efficiency expectations observed from the static-pressure and heat-transfer data. The assumption of uniform reaction efficiency must result in some distortion of the temperature profiles from the real flow. (The E_r values were selected so that the combustion efficiency value deduced from the integral computation was equal to the one-dimensional analysis values.) In reality, one would expect higher combustion efficiency in fuel-lean regions because of the availability of excess oxygen; however, in the absence of probe or other data which correctly defined the combustion efficiency distribution, local η_c (or E_r) could not be uniquely determined. As noted in the one-dimensional analysis result, comparisons between the one-dimensional computation and the integral computations substantiate the consistency of the data analysis procedures.

One-Dimensional Analysis

Wall static pressure.- The static-pressure distribution computed by use of the one-dimensional analysis program for $\phi = 0$ is presented in figure 7 for the Q_3 and Q_1 configurations and in figure 8 for the A_x configuration. The computation is in good agreement with the data until flow separation occurs, with the exception of shock-related pressures not treated by the analysis.

The curve in figure 12 labeled one-dimensional computation, $\phi = 0.88$, was computed by using a mixing efficiency correlation for normal injection reported

12

in reference 11. The general correlation (fig. 1 of ref. 11) expresses the mixing efficiency as a function of length x divided by the length required for complete reaction. Empirical knowledge is used to select the latter length scale. For the computation shown, the length scale criterion was chosen for consistency with the scramjet module design, where a mixing efficiency of 95 percent is specified at a distance of 48 strut gaps from the injection region. By using this criteria for the two-dimensional step model, which has a length of approximately 20 strut gaps, the mixing efficiency at the model exit is about 82 percent which is in good agreement with the experimental data values of 79 to 83 percent. (See table II.) Since the values of mixing efficiency used in the one-dimensional computation correspond well with the data, differences between the computed and data pressure distribution are principally due to the assumption $\eta_m = \eta_c$ used in the one-dimensional analysis; that is, combustion is not proceeding at as rapid a rate as mixing as implied by the assumption $\eta_m = \eta_c$.

Heat-transfer distributions.- Heat-transfer distributions were computed by using the one-dimensional analysis program in conjunction with the data fairings from figures 7, 8, 12, 13, and 14. The distributions are presented in figures 16, 17, and 18 for the Q_3, Q_1, and A_x configurations, respectively. The distributions are considered to be a good representation of the data.

Combustion efficiency distributions.- Combustion efficiency distributions for the three configurations are presented in figure 28 for the $\phi = 0.5$ data and in figure 29 for the $\phi = 0.9$ data. The efficiencies presented have been scaled by the ratio of the local injected hydrogen to the total injected hydrogen, which provides a continuous distribution throughout the injection region. Without this scaling factor, an apparent drop in efficiency would occur at the second-stage injection station because of the sudden increase in hydrogen mass flow. The distributions for the Q_3 and Q_1 configurations and both equivalence ratios (figs. 28 and 29) increase monotonically from the location of the fuel injectors until larger area divergence occurs near x = 27 cm. In this region (27 < x < 37 cm), η_c becomes relatively constant and then increases to the exit values. The constant region is indicative of little or no reaction and suggests the expansion of the flow suppresses the reaction, that is, the rate of expansion dominates effects due to the rate of reaction.

In contrast, the η_c distribution for the A_x configuration and both equivalence ratios increases more rapidly near the injectors than for both the Q_3 and Q_1 configurations. In the downstream region, x > 37 cm, the rate of reaction, as reflected in the slope of the η_c curve, is slower for the A_x configuration than for the Q_3 and Q_1 configurations. The more rapid increase in η_c near the injectors is probably due to less flow expansion (smaller wall angles) and better distribution of the fuel due to the use of more and smaller injection orifices promoting more rapid mixing and ignition. The less rapid increase in η_c in the downstream region for the A_x configuration, relative to the Q_3 and Q_1 configurations, may be due to the stratification of the fuel (fig. 21) producing a flow two-dimensional in nature and thus slower to mix than the highly three-dimensional fuel contours of the Q_3 and Q_1 configurations. (Refer to figs. 19 and 20.) In addition, the larger expansion angle of the A_x configuration in the downstream region (fig. 3) may have had an adverse effect on the combustion process. The absence of the nearly constant

region in the A_x configuration is probably due to rapid initial reaction increasing the temperature sufficiently previous to the downstream expansion so that the reaction-generated pressure rise dominates the effect of the area expansion.

The computed pressure distribution presented in figure 15 for the reduced temperature test was computed by Waltrup (ref. 12) by using the method of reference 17. This analysis takes account of a precombustion shock if the pressure rise at the injectors is sufficiently high to separate the boundary layer. The deduced combustion efficiency of 60 percent is of comparable magnitude to the higher temperature A_x configuration data of 58 percent. As the upstream separation precludes this mode of injection for an operational scramjet, the data substantiate the need to tailor fuel injection between normal and parallel modes to prevent undesirable separation when operating over a Mach number regime as noted in reference 1.

Mixing, combustion, and reaction efficiencies.- The parameters which best express the overall performance of the test configurations are mixing, combustion, and reaction efficiencies. (See figs. 28 and 29 at the model exit of $x = 78.7$ cm, also table II.) Combustion efficiencies for the Q_3, Q_1, and A_x configurations for $\phi = 0.5$ are 0.63, 0.55, and 0.64, respectively. As no probe data were available to determine mixing efficiencies for $\phi = 0.5$, the reaction efficiencies could not be determined.

Combustion efficiencies for the $\phi = 0.9$ data were 0.42 for the Q_3 and Q_1 configurations and 0.58 for the A_x configuration. By using the mixing efficiency values deduced from the probe data of 83 percent for the Q_3 configuration and 79 percent for the Q_1 and A_x configurations, the reaction efficiency is 51 to 53 percent for the Q_3 and Q_1 configurations and 74 percent for the A_x configuration. The significance of these parameters is that although approximately 80 percent of the hydrogen fuel was mixed so that it could react, only approximately 50 percent of the mixed fuel reacted in the Q_3 and Q_1 configurations. Somewhat better reaction (74 percent) occurred in the A_x configuration. Clearly, these results indicate much poorer reaction than can be tolerated in a practical combustor, and that the combustor performance of the model was reaction limited as opposed to mixing limited.

One immediate conclusion from the Q_3 and Q_1 configuration data is that the ratio of fuel dynamic pressure to free-stream dynamic pressure does not have a significant effect upon the combustion efficiency of the model. For the current Q_3 configuration tests, the dynamic pressure ratios for the top and bottom injectors were 2.45 and 2.13, respectively. Similarly, for the Q_1 configuration, the fuel dynamic pressure ratios were 0.81 and 0.79 for the top and bottom injectors, respectively. Previously conducted flat-plate cold nonreacting mixing data indicated an increase in penetration and thus mixing with increasing ratio of injectant dynamic pressure to free-stream dynamic pressure. (See ref. 18.) However, in the cold mixing tests a higher dynamic pressure ratio was accompanied by increasing mass flow of injectant. For the current reacting flow tests, the constraint of a fixed mass flow of injectant (hydrogen) is an additional restriction which requires the variation of dynamic pressure to be accomplished by changes in orifice diameter. Comparative results herein are therefore between a high dynamic pressure ratio and small orifice and a low

dynamic pressure ratio and large orifice; effects which tend to offset each other. Also, the results of reference 18 were not affected by injection from an opposite wall.

Comparison of One-Dimensional and Integral Programs

Comparative results between the one-dimensional and integral programs are presented in table II for $\phi = 0.9$. The two computations are not entirely independent due to the use of η_c from the one-dimensional analysis in the integral program computation. However, the reasonable agreement in values of total enthalpy, thrust function, and mass flow substantiates the consistency of the analysis techniques. Note that the total mass flow W, computed from the survey data, is 10, 11, and 4 percent low for the Q_3, Q_1, and A_x configurations, respectively. When the quantity of the data measurements involved in making the computation is considered, agreement within 10 percent is considered good. The poorer agreement for the Q_3 and Q_1 configurations is attributed to attempting to describe a complex three-dimensional flow with a limited number of data points, as opposed to the A_x configuration exit profiles, which were more uniform and relatively two-dimensional in nature.

Local Fuel Injection Effects

The previously presented data indicate the combustion efficiency of the two-dimensional step model to be more reaction limited than mixing limited. The poor penetration of the bottom injectors is believed to be a significant factor affecting the combustion efficiencies of the Q_3 and Q_1 configurations. Pressure disturbances associated with the upstream injectors are related to the poor penetration of the downstream bottom injectors as described in the following paragraphs. (Also, see ref. 12.)

Figure 30 presents the difference in static pressure on the fuel injector blocks measured by static taps located downstream and also between the injection orifice locations. The relative location of the pressure taps is illustrated at the top of figure 30. The fuel equivalence ratio schedule for the data presented is also tabulated in the figure. Note that the curves shown are related through the fuel injection schedule. Note positive Δp indicates low pressure downstream of the injection orifices relative to the pressure between the orifices. The data corresponding to the top fuel injector block (circle symbols in fig. 30) are considered to be typical behavior for normal injection, as blockage due to injection causes a low pressure recirculation region to occur downstream of the orifice, and generally increase with increasing fuel injection (increasing ϕ). Of course, this distribution is independent of the bottom fuel injection which is located further downstream. For bottom injection only, the data point labeled $\phi_t = 0.0$, $\phi_b = 0.3$ indicates the bottom injector block pressures are consistent with the top injector block pressures.

In contrast to the top injector, the bottom injector experienced a reduction in the pressure difference from the in-line and between orifice pressures with increasing fuel injection as evidenced by the curve labeled "bottom injector" in figure 30. The pressure reduction is believed to be due to the

pressure distribution imposed on the bottom injection block by fuel injection from the top injector. The data point labeled "$\phi_b = 0.0$, $\phi_t = 0.44$" supports this contention, as the top injection imposed a relatively high pressure region (negative Δp) in the proximity of the bottom injection orifices as evidenced by the static tap immediately downstream of the bottom injector. Note the magnitude of this pressure difference is nearly equal to the magnitude of the pressure difference on the top injector block for the same ϕ but of opposite sign. This imposed pressure difference was apparently too strong for the bottom injection process to overcome and, as a result, there was poor penetration from the bottom injectors. The poor penetration was undoubtedly accompanied by reduced shock strengths and/or significantly modified shock structure relative to that associated with good penetrating jets. Shocks associated with the injection process can be significant in initiation of the combustion process by increasing the temperature; hence, a plausible relation between poor penetration and poor combustion. The effect of the shocks is expected to be most significant for static temperatures near the autoignition temperature (approximately 1000 K for hydrogen-air mixture) and it is noted in the current tests that the static temperature was not significantly greater (1060 K).

RECOMMENDATIONS

Numerous factors can affect the reaction efficiency of the combustion process. Effects which need to be systematically addressed in future tests are the following: hydrogen fuel temperature, model wall temperature, test-gas temperature, flow expansion angle, injector size, spacing, and attitude. The effect of the flow expansion angle was partially examined in the current tests by reducing the wall angles near the injectors in the A_x configuration; however, the wall angle change was accompanied by changes in the injector geometry and injection orifices and thus wall angle and injection effects could not be entirely separated. However, the better reaction efficiency of the A_x configuration as opposed to the Q_3 and Q_1 configurations suggests an expansion effect. One-dimensional-analysis results of the Q_3 and Q_1 configuration data (although limited because of problems in attempting to describe a three-dimensional flow with a one-dimensional analysis) also suggest that if the reaction has not caused significant temperature rise prior to expansion of the flow, the reaction may be suppressed (quenched).

Injector spacing, which affects reaction through both the resulting shock structure and mixing rates, was reported (ref. 12) to be near optimum at a value equal to the combustor entrance height of 3.89 cm. This is consistent with the data as the A_x configuration employed six orifices at a spacing of 2.83 cm and undesirable flow stratification occurred; therefore, the spacing was too close. Configurations Q_3 and Q_1 employed four orifices in the top injector at a spacing of 4.25 cm without undesirable stratification. This suggests four to five injectors (spacing 4.25 to 3.4 cm) to be near optimum for the current model. Future tests should employ four injection orifices, and although the effects of the fuel dynamic pressure ratio were not identifiable in the current tests, pure scale considerations suggest high fuel dynamic pressure ratios (small orifices) are desirable to minimize mixing lengths.

16

One other factor affecting the penetration and mixing, but probably to a small degree, is related to the injection orifice locations. They were positioned 2.3 step heights downstream of the steps with the belief that they would still be ahead of the flow attachment location. However, heating patterns on the top injector of the Q_3 configuration indicated reattachment occurred approximately at the injection orifices. Some improvement in penetration may be achieved by repositioning the orifices closer to the step within the low pressure unattached flow regime.

Further experimental work should be conducted to establish criteria necessary to eliminate the adverse fuel injection effects. These tests should also consider relocation of the injection orifices closer to the steps, in-line as opposed to interdigitated injectors, angled as opposed to normal injection, and variation of the relative longitudinal location of the fuel injection orifices. The latter variation will change the location at which the upstream injection disturbance interacts with the lower injection region. Insufficient data were acquired to define the highly complex interactions due to fuel injection or to determine whether the imposed pressures are primarily disturbance effects or both disturbance- and combustion-related effects. These effects could be separated by subsequent tests by using helium to replace the hydrogen fuel or by elimination of oxygen from the facility test gas.

Further experiments are also needed to examine the effect of the length scale of the model. The current model length-height ratio (model entrance height) of approximately 20 from the injectors to the duct exit compares with a value of 48 for the currently envisioned scramjet modules. Therefore, some consideration must be given as to what would happen to the mixing and reaction rates if the exit profiles were allowed to continue to expand; for example, if the model were extended to the scale length of the scramjet module. Previously reported results (ref. 12) indicated mixing efficiencies of 95 percent should be attainable in the scramjet module design where the additional length is provided. This observation should be addressed both experimentally by extending the model length and analytically by use of three-dimensional mixing and reacting codes currently under development. (For example, see refs. 19 and 20.) Based upon consideration of the gradients in the exit flow for the configurations tested, it is believed the more three-dimensional profiles of the Q_3 and Q_1 configurations will continue to mix at a faster rate than the more stratified flow of the A_x configuration.

Data analysis, although providing significant information on the performance of the model was seriously impaired by the inability of the sample probe to quench the sample. Complete quenching will probably never be achieved; however, top priority to probe tip redesign and finite-rate kinetic computational analysis and experimental verification should result in substantial improvement in future data.

CONCLUDING REMARKS

An investigation of the combustion of hydrogen perpendicularly injected from step fuel injectors into a Mach 2.72, 2100 K vitiated test gas has been conducted. Three test configurations were employed; the first two were used

to determine the effect of varying the fuel dynamic pressure ratio, and the third configuration was evolved in an attempt to improve the combustion efficiency relative to the other configurations. The two-dimensional model simulated the flow between the center and side struts of an integrated scramjet module. Significant results and recommendations follow.

No measurable improvement in mixing efficiency or combustion efficiency was obtained by varying the fuel to test stream dynamic pressure ratio from 0.79 to 2.45.

Consistent with earlier reported results, injector spacing equal to model entrance height is near optimum for best mixing. Although not substantiated experimentally, scale considerations suggest the use of high dynamic pressure ratio (small orifices) for injection.

For the three configurations tested, approximately 80 percent of the injected fuel was mixed within the model length, which corresponds to 5/12ths of the scale length of currently envisioned scramjet modules. Further tests and three-dimensional flow analysis capability should be used to determine the downstream mixing rate.

Although 80 percent of the injected fuel was mixed so that it could react, only 51, 53, and 74 percent of the mixed fuel actually reacted in the three configurations tested. The reason for the poor reaction (51 to 53 percent) is believed to be associated with adverse pressure disturbances associated with the upstream injectors impinging upon the downstream injection region. The adverse pressure resulted in poor penetration of fuel from the downstream injectors. Better reaction (74 percent) was achieved by area distribution reduction (less expansion) and increasing the number of fuel injectors, the latter at the expense of poorer penetration and undesirable stratification of the fuel.

Combustion efficiency distributions deduced from wall pressure measurements by use of a one-dimensional analysis suggest that if the reaction is not sufficiently initiated prior to flow expansion, the reaction may be suppressed (quenched). This result emphasizes the need to design for rapid ignition and to be able to predict the result of flow expansion upon the reaction process.

Consistent agreement between one-dimensional analysis using the wall static-pressure data and integral analysis of the probe pitot pressure and gas composition measurements was obtained. However, the inability of the sample probe to quench the reaction prevented accurate determination of local combustion efficiency. Therefore, priority should be given to probe redesign and subsequent experimental verification of the shock swallowing and quenching capabilities of the new probe during gas sample collection.

Langley Research Center
National Aeronautics and Space Administration
Hampton, VA 23665
April 4, 1978

REFERENCES

1. Henry, John R.; and Anderson, Griffin Y.: Design Considerations for the Airframe-Integrated Scramjet. NASA TM X-2895, 1973.

2. Beach, H. L., Jr.: Supersonic Mixing and Combustion of a Hydrogen Jet in a Coaxial High-Temperature Test Gas. AIAA Paper No. 72-1179, Nov.-Dec. 1972.

3. Evans, John S.; and Anderson, Griffin Y.: Supersonic Mixing and Combustion in Parallel Injection Flow Fields. Analytical and Numerical Methods for Investigation of Flow Fields With Chemical Reactions, Especially Related to Combustion. AGARD CP-164, Apr. 1974, pp. III3-1 - III3-8.

4. Rogers, R. C.; and Eggers, J. M.: Supersonic Combustion of Hydrogen Injected Perpendicular to a Ducted Vitiated Airstream. AIAA Paper No. 73-1322, Nov. 1973.

5. Russin, Wm. Roger: The Effect of Initial Flow Nonuniformity on Second-Stage Fuel Injection and Combustion in a Supersonic Duct. NASA TM X-72667, 1975.

6. Bahr, D. W.; Kenworthy, M. J.; Hoelmer, W.; and King, R. C.: Scramjet Exploratory Development Program. NASA CR-1502, 1970.

7. Billig, F. S.; Orth, R. C.; and Funk, J. A.: Direct-Connect Tests of a Hydrogen-Fueled Supersonic Combustor. NASA CR-1904, 1971.

8. Hypersonic Research Engine Project - Phase II. Combustor Program. Rep. No. AP-70-6054 (Contract NAS1-6666), Airesearch Manufacturing Div., The Garrett Corp., Mar. 23, 1970. (Available as NASA CR-66932.)

9. McClinton, Charles R.; Torrence, Marvin G.; Gooderum, Paul B.; and Young, Irene G.: Nonreactive Mixing Study of a Scramjet Swept-Strut Fuel Injector. NASA TN D-8069, 1975.

10. Anderson, Griffin Y.; and Gooderum, Paul B.: Exploratory Tests of Two Strut Fuel Injectors for Supersonic Combustion. NASA TN D-7581, 1974.

11. Anderson, Griffin Y.: An Examination of Injector/Combustor Design Effects on Scramjet Performance. NASA paper presented at the 2nd International Symposium on Air Breathing Engines (Sheffield, England), Mar. 25-29, 1974.

12. Anderson, Griffin Y.; Eggers, James M.; Waltrup, Paul J.; and Orth, Richard C.: Investigation of Step Fuel Injectors for an Integrated Modular Scramjet Engine. 13th JANNAF Combustion Meeting, Volume III, CPIA Publ. 281 (Contract N00017-72-C-4401), Appl. Phys. Lab., Johns Hopkins Univ., Dec. 1976, pp. 175-189.

13. Engineering Analyses and Design Calculations of NASA Langley Research Center Hydrogen-Air-Vitiated Heater With Oxygen Replenishment. Tech. Memo. No. 173, Gen. Appl. Sci. Labs., Inc., 1974. (Available as NASA CR-132381.)

14. Russin, William Roger: Performance of a Hydrogen Burner To Simulate Air Entering Scramjet Combustors. NASA TN D-7567, 1974.

15. Eggers, James M.: Composition Surveys of Test Gas Produced by a Hydrogen-Oxygen-Air Burner. NASA TM X-71964, 1974.

16. Pinckney, S. Z.: Turbulent Heat-Transfer Prediction Methods for Application to Scramjet Engines. NASA TN D-7810, 1974.

17. Billig, F. S.; and Dugger, G. L.: The Interaction of Shock Waves and Heat Addition in the Design of Supersonic Combustors. Twelfth Symposium (International) on Combustion, Combust. Inst., c.1969, pp. 1125-1139.

18. Rogers, R. Clayton: Mixing of Hydrogen Injected From Multiple Injectors Normal to a Supersonic Airstream. NASA TN D-6476, 1971.

19. Zelazny, S. W.; Baker, A. J.; and Rushmore, W. L.: Modeling of Three-Dimensional Mixing and Reacting Ducted Flows. NASA CR-2661, 1976.

20. Dyer, D. F.; Maples, G.; and Spalding, D. B.: Combustion of Hydrogen Injected Into a Supersonic Airstream (A Guide to the Hiss Computer Program). NASA CR-2655, 1976.

TABLE I.- TEST CONDITION SUMMARY

Test	$P_{t,h}$, MN/m^2	$T_{t,h}$, K	ϕ_t	ϕ_b	ϕ
Configuration Q$_3$					
427-1	2.88	2120	0.0	0.0	0.0
427-4	2.90	2090	.23	.19	.4˙
425-11	2.94	2060	.46	.44	.90
427-3	2.91	2150	.47	.41	.88
425-10	2.91	2070	.46	.38	.84
426-4	2.90	2060	.47	.41	.88
427-2	2.89	2060	.46	.42	.88
Q$_3$ average	----	----	.46	.41	.87
Configuration Q$_1$					
428-9	2.89	2060	0.0	0.0	0.0
428-5	2.94	2140	.24	.24	.48
428-8	2.94	2090	.46	.45	.91
428-10	2.92	2030	.47	.46	.93
428-7	2.92	2110	.47	.43	.90
428-11	2.91	2160	.49	.46	.95
428-12	2.94	2130	.47	.45	.92
Q$_1$ average	----	----	.47	.45	.92
Configuration A$_x$					
435-1	2.95	2130	0.0	0.0	0.0
435-3	2.92	2100	.23	.20	.43
435-4	2.92	2090	.52	.48	.90
435-6	2.89	2100	.49	.42	.91
435-9	2.92	2100	.48	.39	.87
435-7	2.89	2073	.48	.42	.90
435-10	2.92	2070	.50	.42	.92
A$_x$ average	----	----	.49	.41	.90
Configuration A$_x$, $T_{t,h}$ = 1670 K					
435-11	2.84	1720	0.0	0.0	0.0
435-13	2.82	1670	.59	.43	1.02

TABLE II.- COMPARISON OF DATA, ONE-DIMENSIONAL,

AND EXIT INTEGRATION COMPUTATIONS

Configuration Q_3							
Parameter	$\phi = 0.0$		$\phi = 0.42$		$\phi = 0.87$		
	Data	1-D analysis	Data	1-D analysis	Data	1-D analysis	Exit survey integration
W, kg/sec	3.96	3.96	4.02	4.02	4.07	4.07	3.65
$\bar{Q}$, MJ/sec	0.32	0.31	0.73	0.72	0.83	0.84	----
C_f	----	0.002	----	0.004	----	0.004	----
η_m	----	-----	----	1.00	----	1.00	0.83
E_r	----	-----	----	0.63	----	0.42	0.51
η_c	----	-----	----	0.63	----	0.42	0.42
H_t, MJ/kg	----	3.72	----	5.54	----	7.49	7.61
F/W, N-sec/kg . . .	----	2112	----	2115	----	2136	2082
M_e	----	3.44	----	2.22	----	1.98	----

TABLE II.- Continued

Parameter	$\phi = 0.48$		$\phi = 0.92$		
	Data	1-D analysis	Data	1-D analysis	Exit survey integration
W, kg/sec	4.02	4.02	4.08	4.08	3.65
$\bar{Q}$, MJ/sec	0.71	0.73	0.87	0.89	----
C_f	----	0.004	----	0.004	----
η_m	----	1.00	----	1.00	0.79
E_r	----	0.55	----	0.42	0.53
η_c	----	0.55	----	0.42	0.42
H_t, MJ/kg	----	5.80	----	7.70	7.85
F/W, N-sec/kg . . .	----	2118	----	2161	2115
M_e	----	2.22	----	1.98	----

Configuration Q_1

TABLE II.- Concluded

Parameter	Configuration A_x						
	$\phi = 0.0$		$\phi = 0.43$		$\phi = 0.90$		
	Data	1-D analysis	Data	1-D analysis	Data	1-D analysis	Exit survey integration
W, kg/sec	3.96	3.96	4.02	4.02	4.08	4.08	3.93
$\bar{Q}$, MJ/sec	0.37	0.33	0.90	0.88	1.02	1.10	----
C_f	----	0.002	----	0.004	----	0.004	----
η_m	----	------	----	1.00	----	1.00	0.79
E_r	----	------	----	0.64	----	0.58	0.74
η_c	----	------	----	0.64	----	0.58	0.58
H_t, MJ/kg	----	3.71	----	5.52	----	7.56	7.61
F/W, N-sec/kg . . .	----	2110	----	2150	----	2254	2230
M_e	----	3.44	----	2.35	----	2.02	----

Parameter	Configuration A_x, $T_{t,h} = 1670$ K	
	$\phi = 0.0$	$\phi = 1.02$
	Data	Data
W, kg/sec	4.32	4.46
$\bar{Q}$, MJ/sec	0.25	1.09
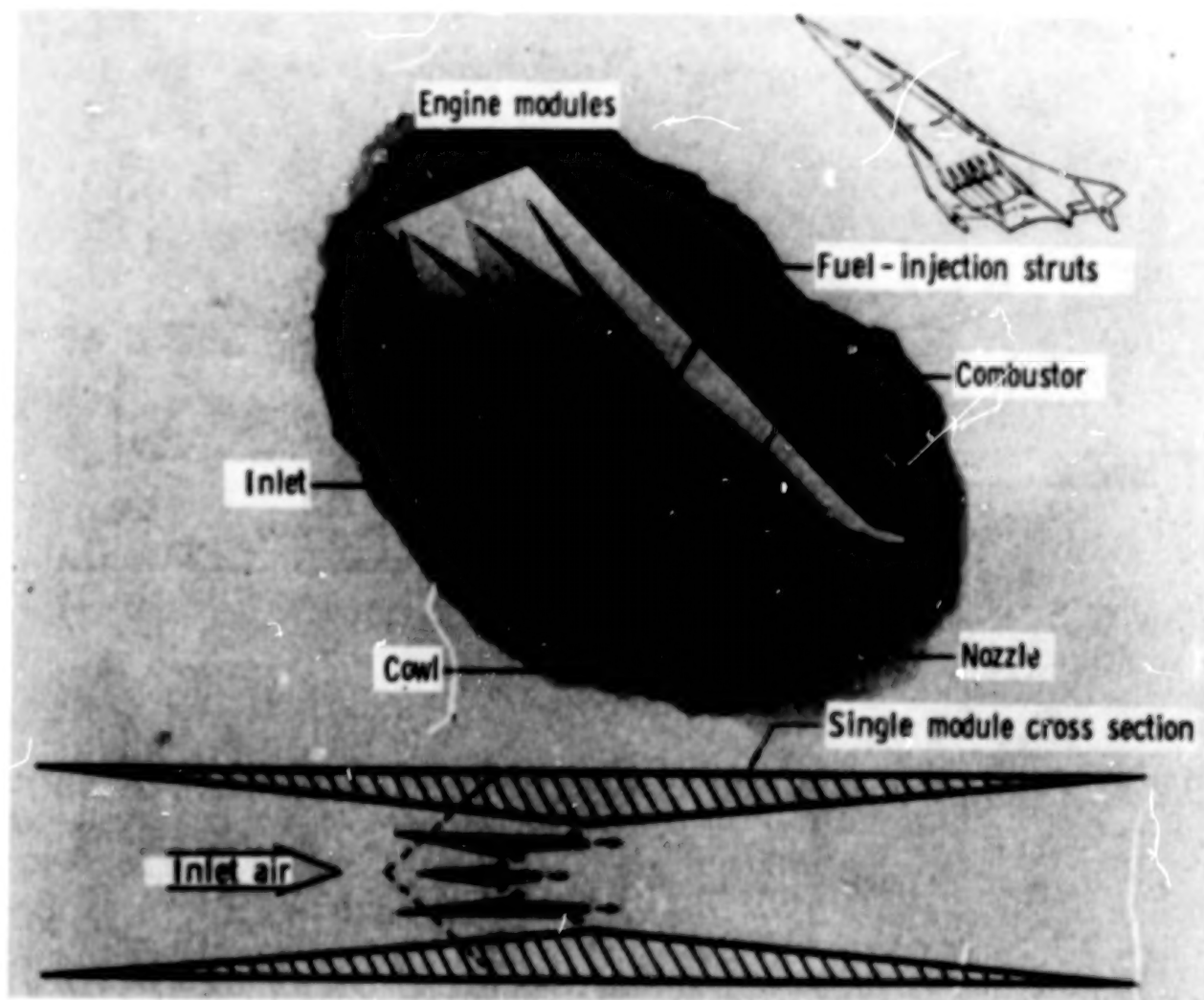
Figure 1.- Airframe-integrated modular scramjet concept.
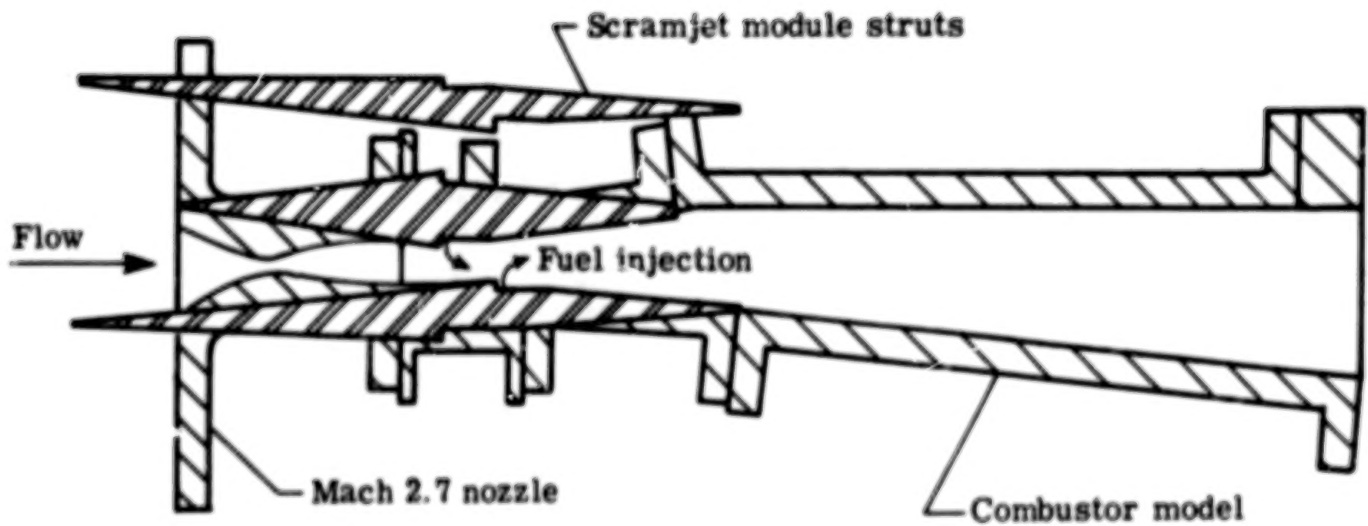
Figure 2.- Model side view illustrating relationship to scramjet module.

Test configuration	δ	β	η	Fuel block identification	
				Top injector	Bottom injector
Q_3	6°	4°	4°	A_t	A_b
Q_1	6°	4°	4°	B_t	B_b
Λ_x	3°	2°	5.1^o	C_t	C_b

▼ Denotes fuel injector locations

Figure 3.- Combustion model details. All dimensions are in centimeters; duct width is constant at 17 cm.
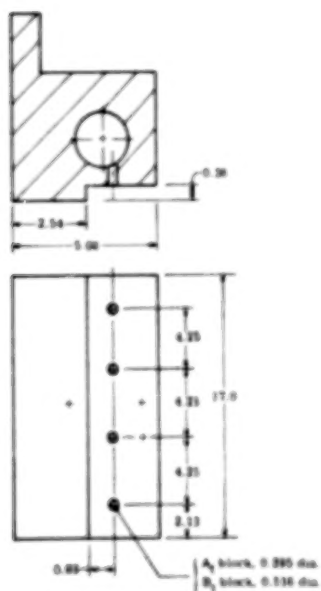
(a) Top fuel injection blocks, A_t and B_t.
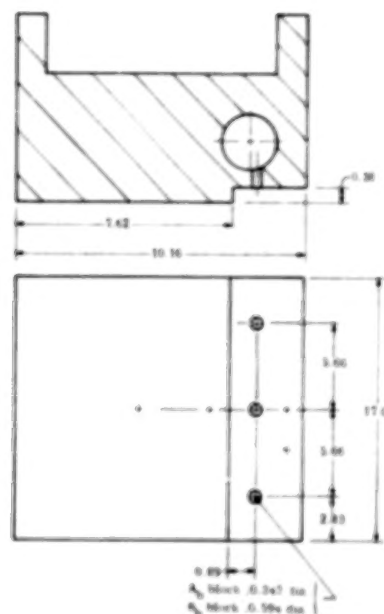
(b) Bottom fuel injection blocks, A_b and B_b.
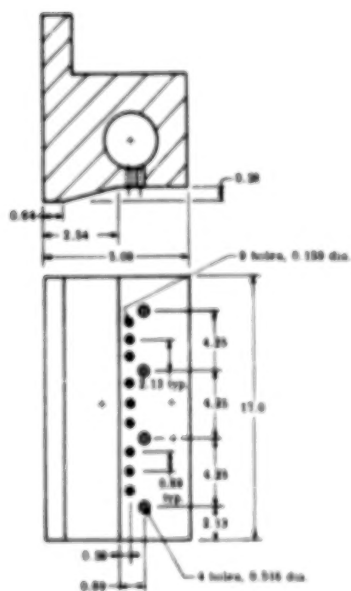
(c) Top fuel injector block, C_t.
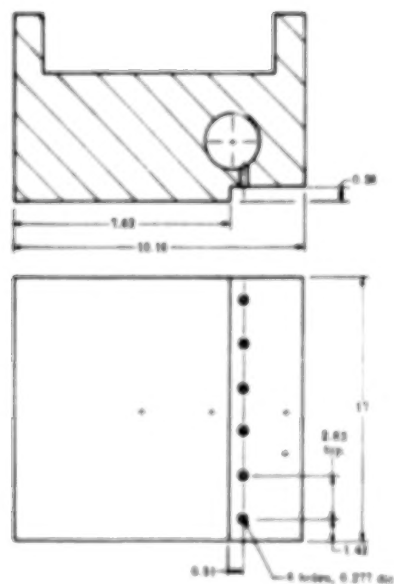
(d) Bottom fuel injector block, C_b.

Figure 4.- Fuel injection block details. All dimensions are in centimeters.

28

Combustion heater

Combustor model

Combustor exit

Survey rake

Exhaust duct

Flow
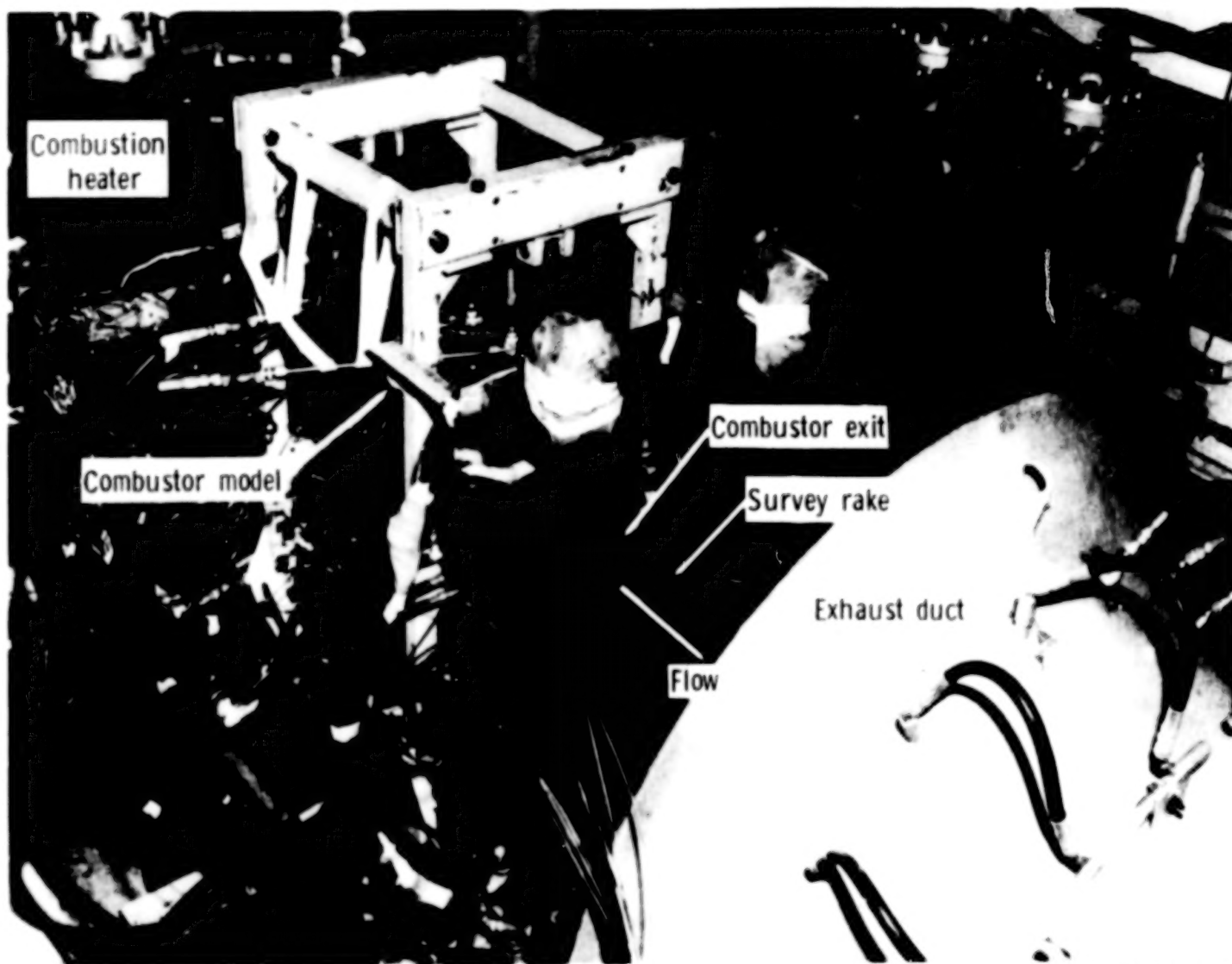
L-74-6053.1

Figure 5.- Combustion duct model installation.
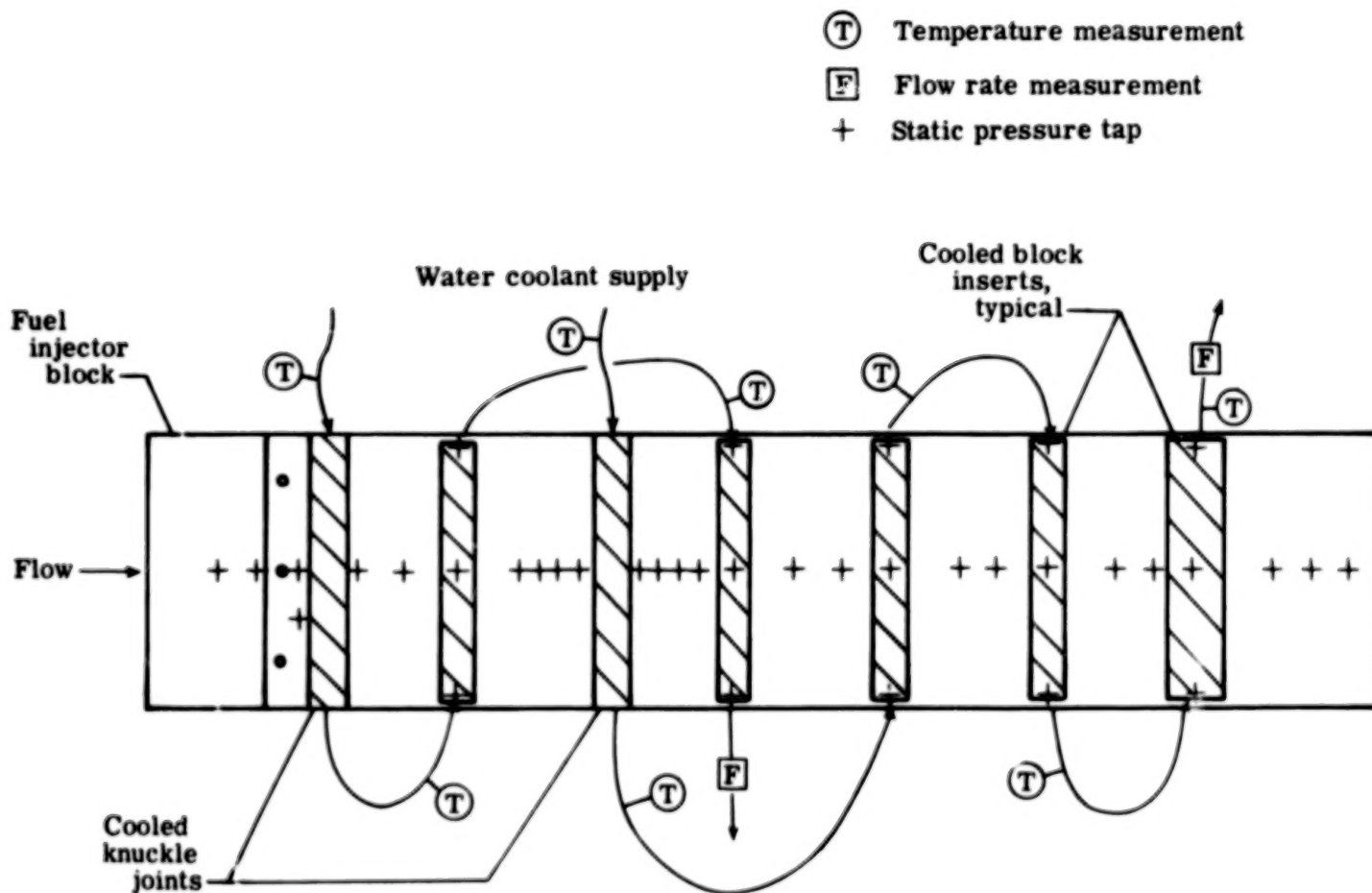
Figure 6.- Bottom surface of combustion model showing typical instrumentation. Top surface is similarly instrumented.
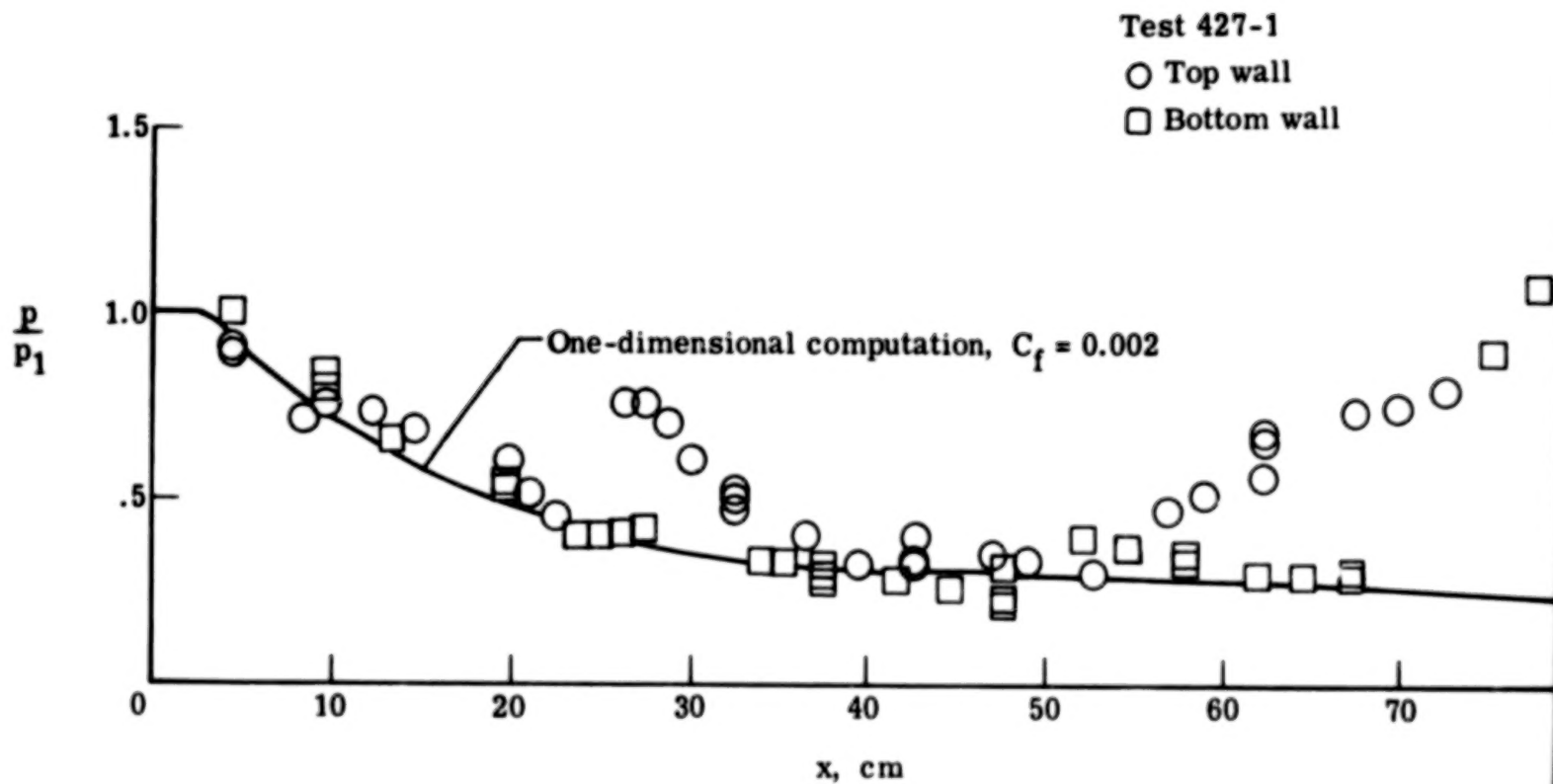
Figure 7.- Wall static-pressure ratio distribution.   Configurations Q_3 and Q_1; $\phi = 0$.

3_1
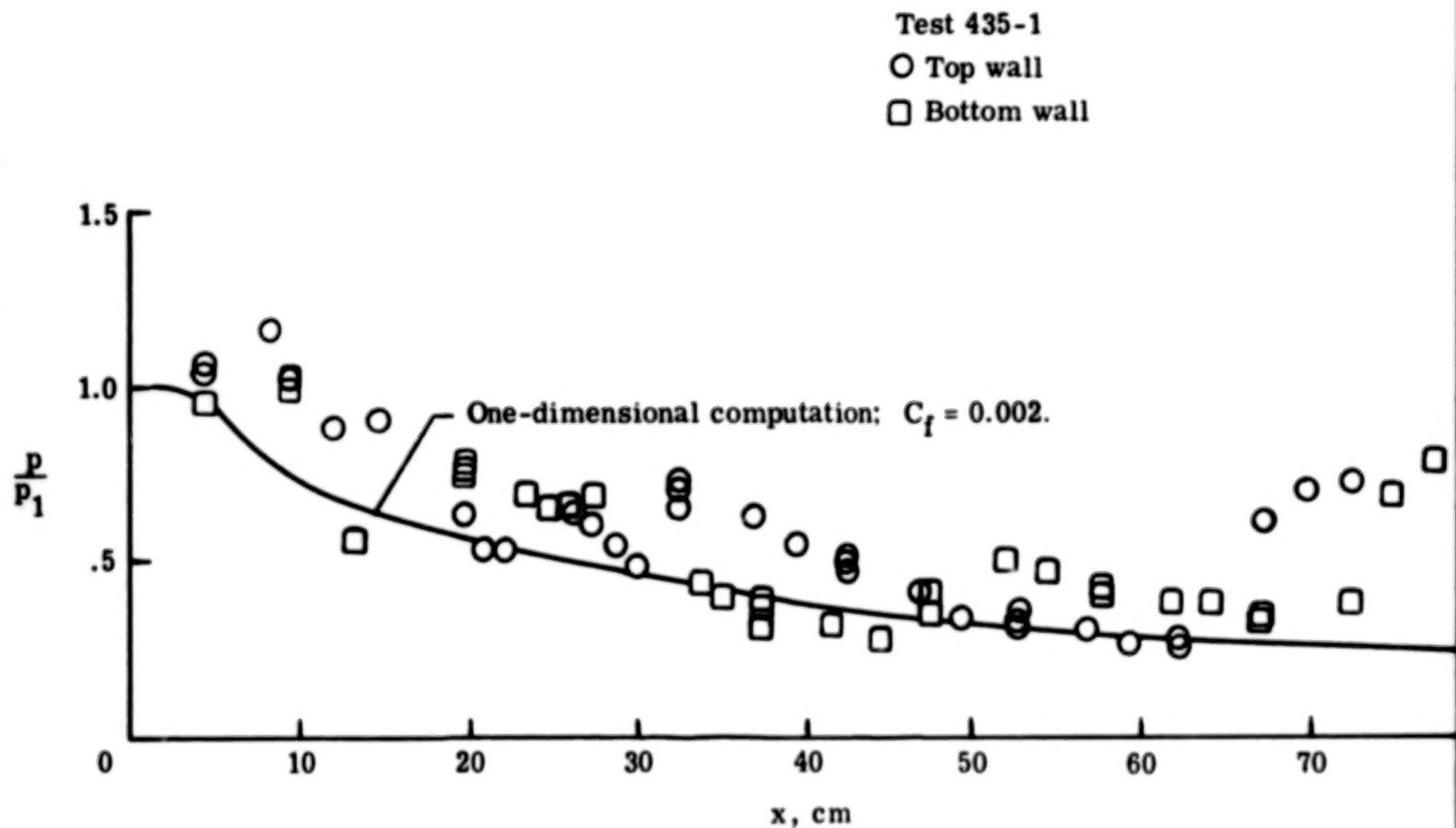
Figure 8.- Wall static-pressure ratio distribution.   Configuration A_x; $\phi = 0$.
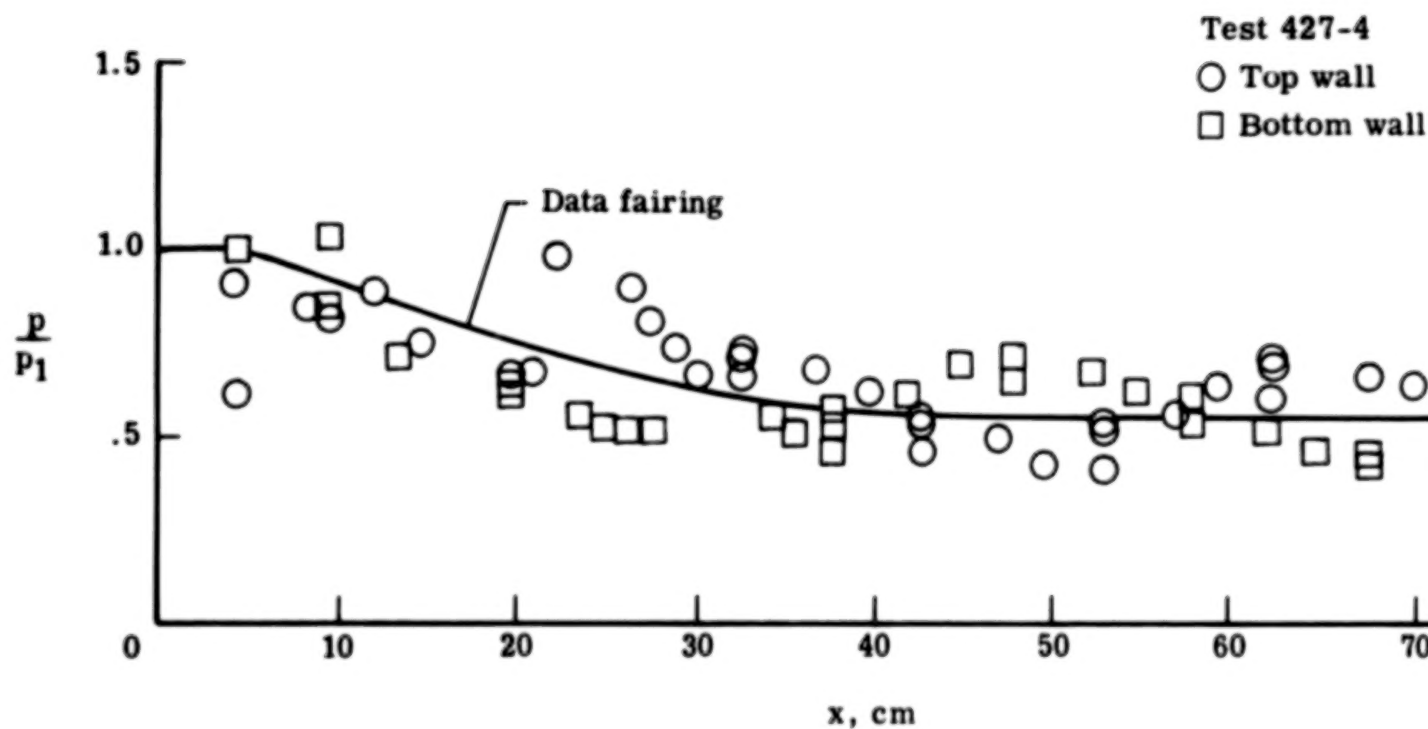
Figure 9.- Wall static-pressure ratio distribution. Configuration Q₃; φ = 0.42.
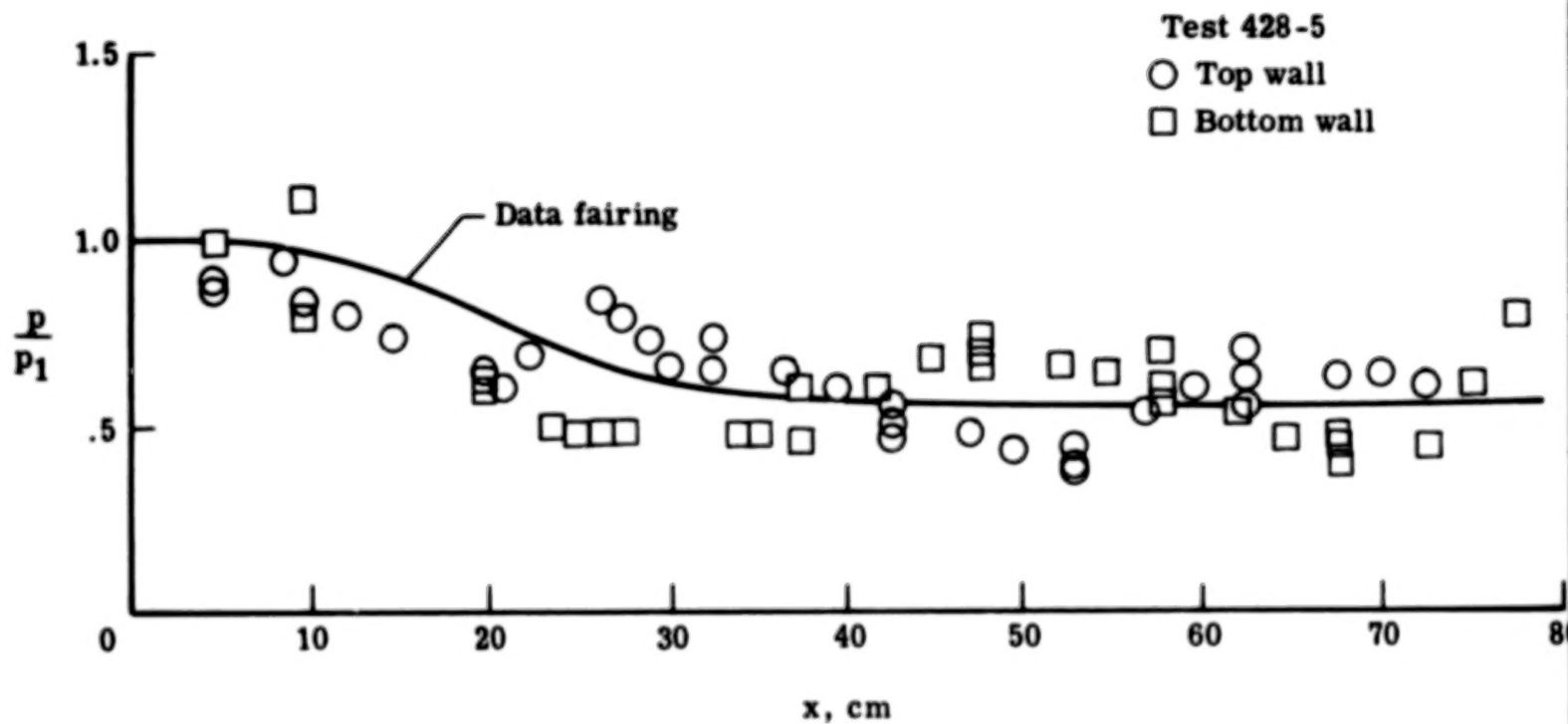
Figure 10.- Wall static-pressure ratio distribution.   Configuration Q_1; $\phi = 0.48$.
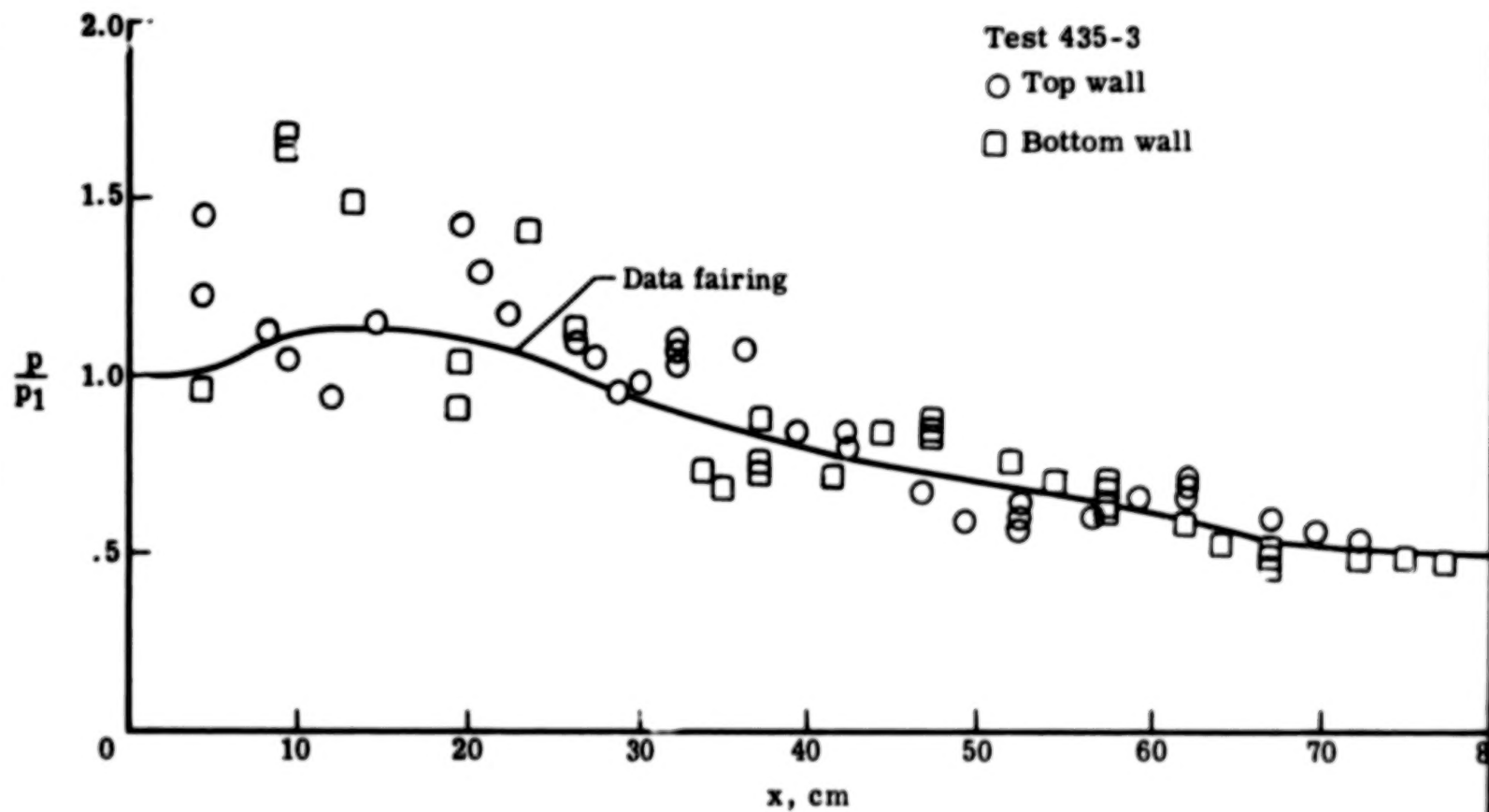
Figure 11.- Wall static-pressure ratio distribution. Configuration A_x; $\phi = 0.43$.
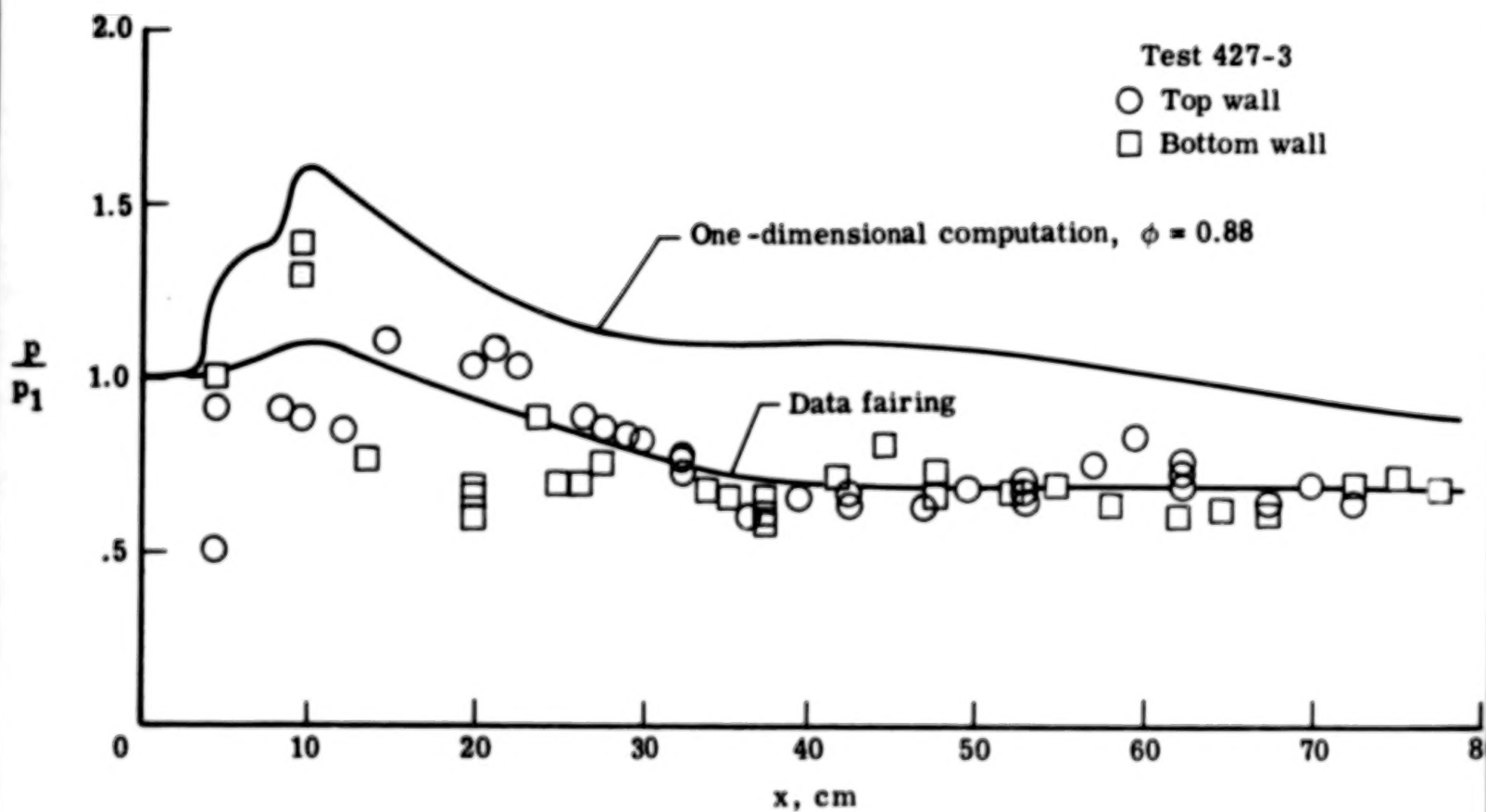
Figure 12.- Wall static-pressure ratio distribution. Configuration Q_3; $\phi = 0.88$.
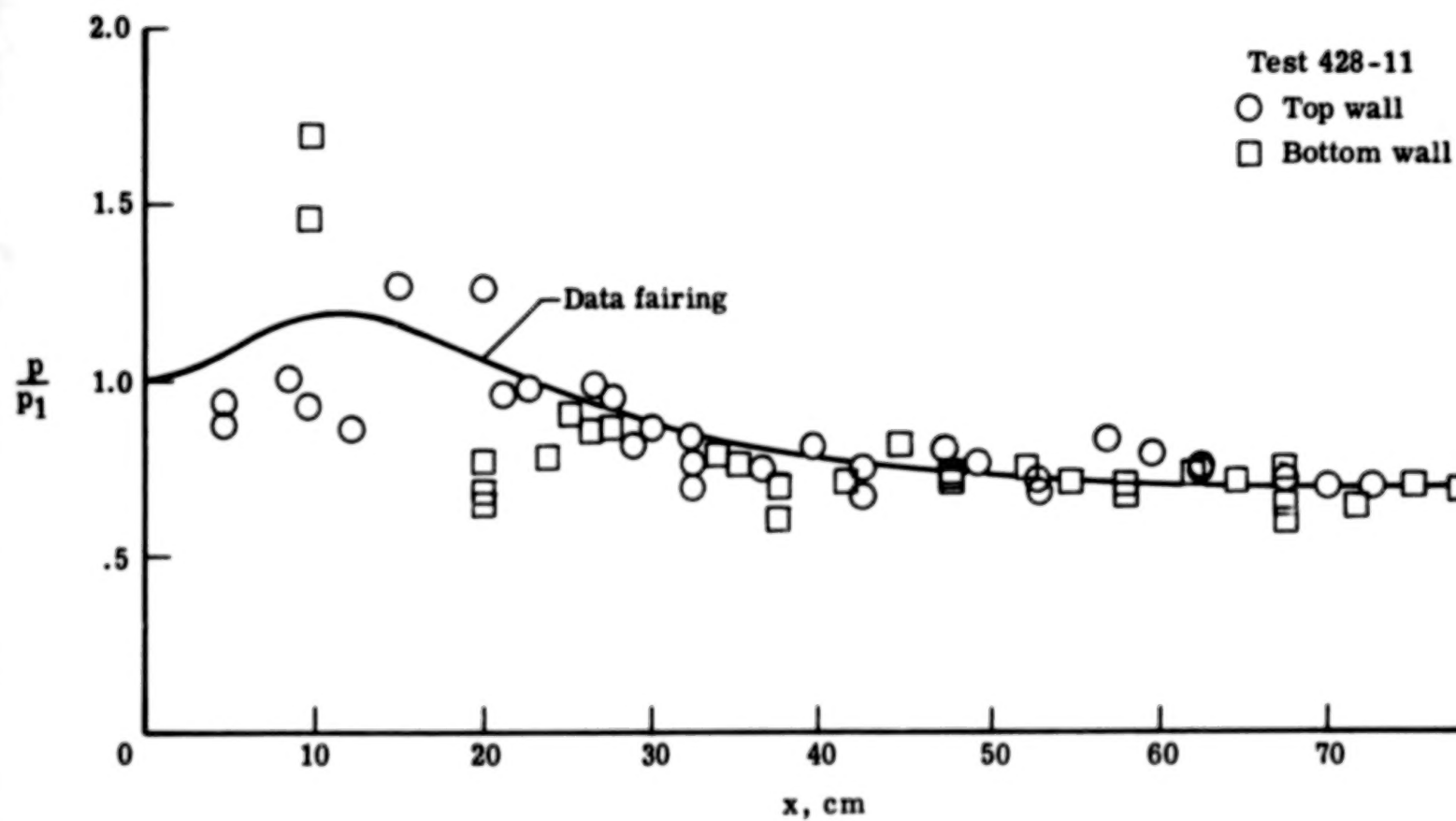
Figure 13.- Wall static-pressure ratio distribution. Configuration Q_1; $\phi = 0.95$.
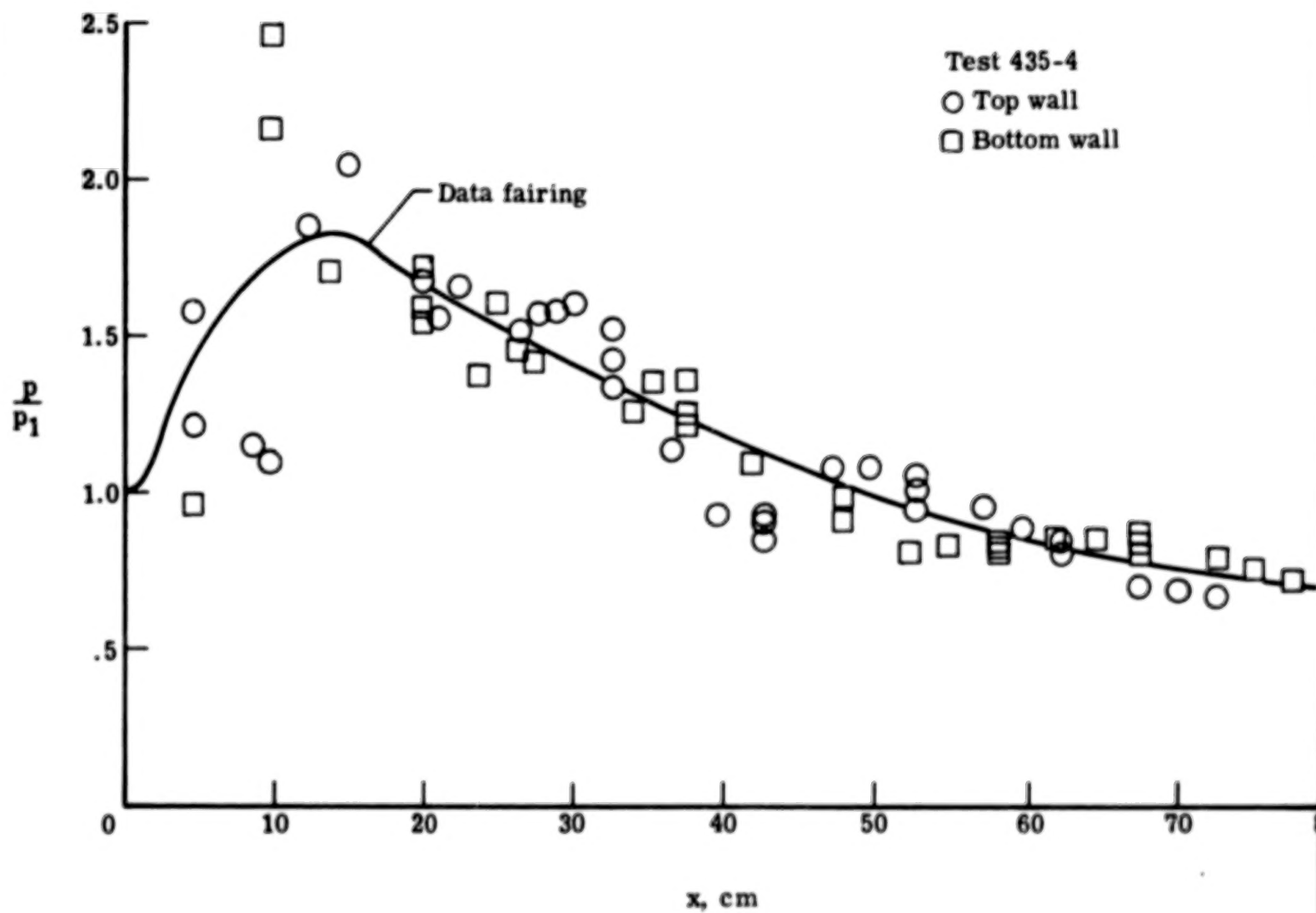
Figure 14.- Wall static-pressure ratio distribution. Configuration A_x; $\phi = 0.90$.
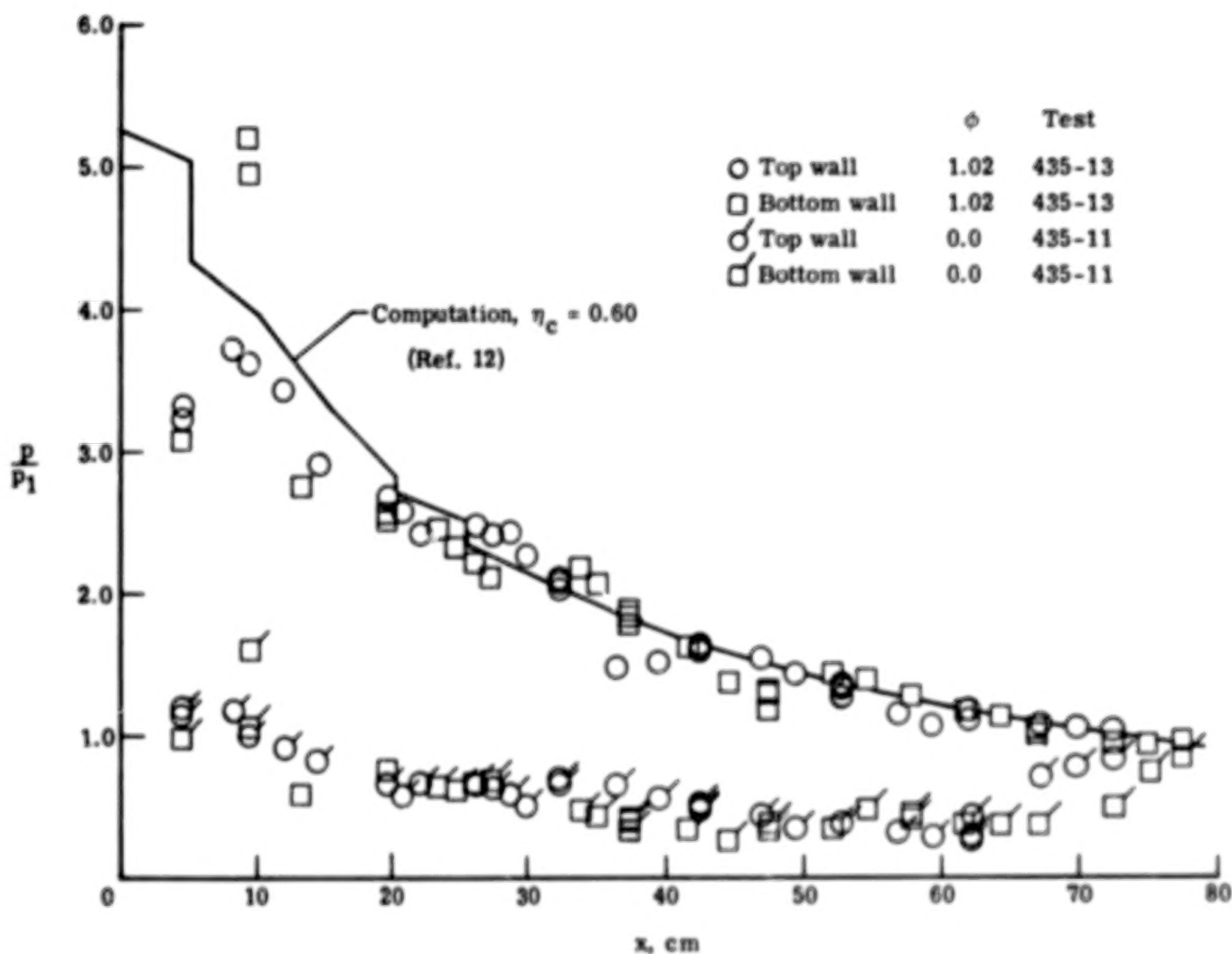
Figure 15.- Wall static-pressure ratio distribution. Configuration A_x; combustion heater at reduced stagnation temperature of 1670 K.
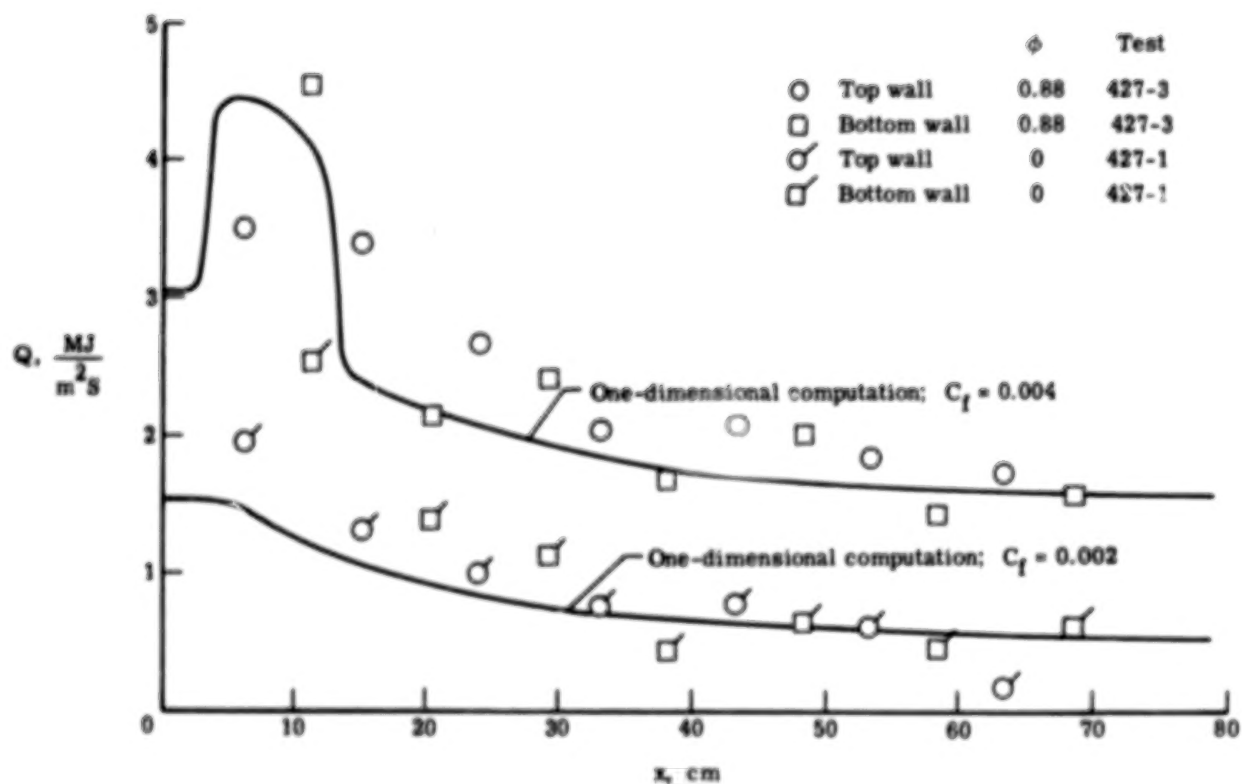
Figure 16.- Wall heat-transfer distribution.   Configuration Q_3; $\phi = 0.88$ and 0.
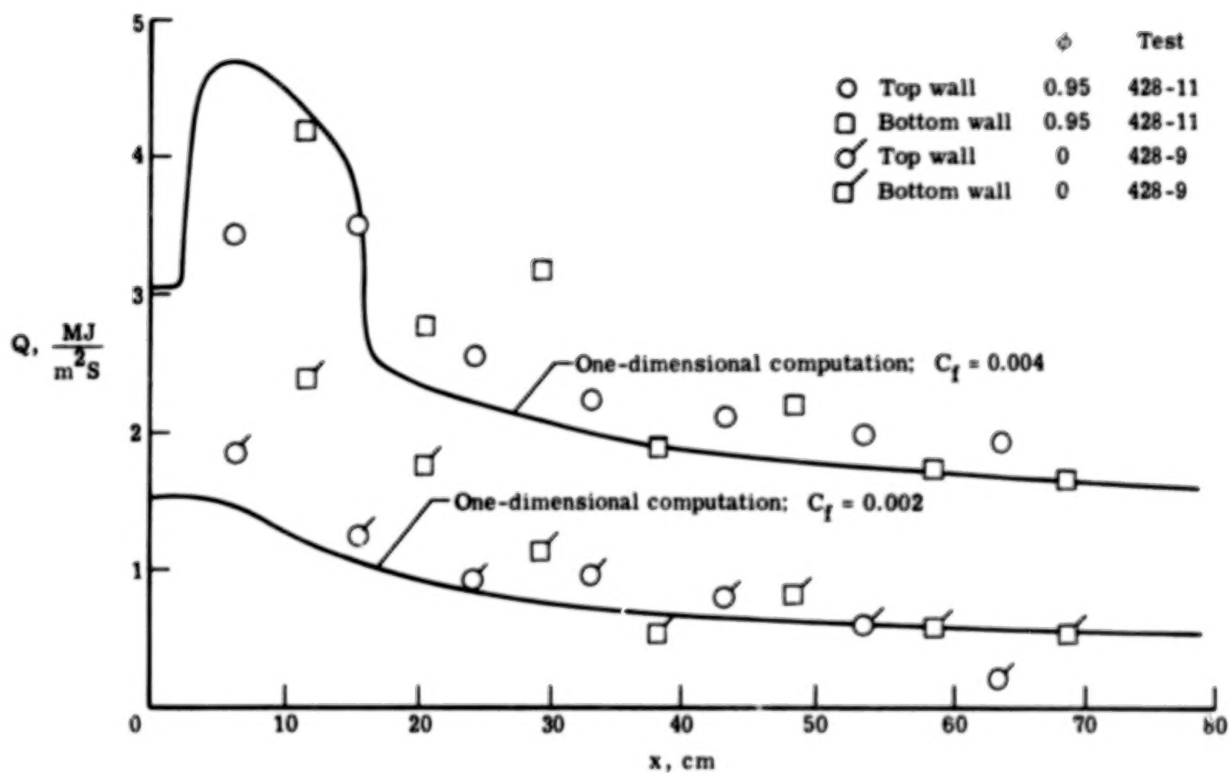
Figure 17.- Wall heat-transfer distribution.   Configuration Q_1; $\phi = 0.95$ and 0.
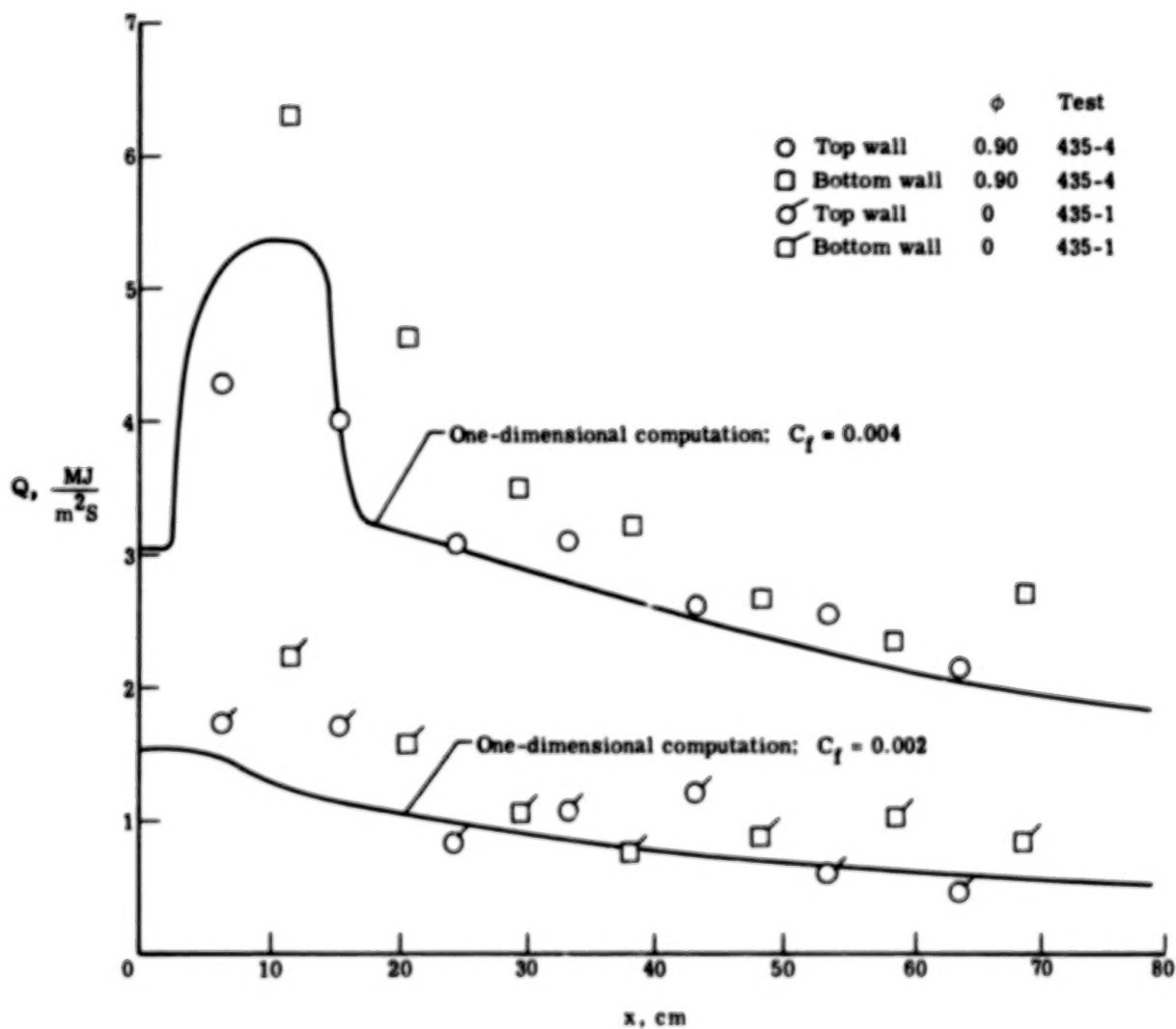
Figure 18.- Wall heat-transfer distribution. Configuration A_x; $\phi = 0.90$ and 0.

42
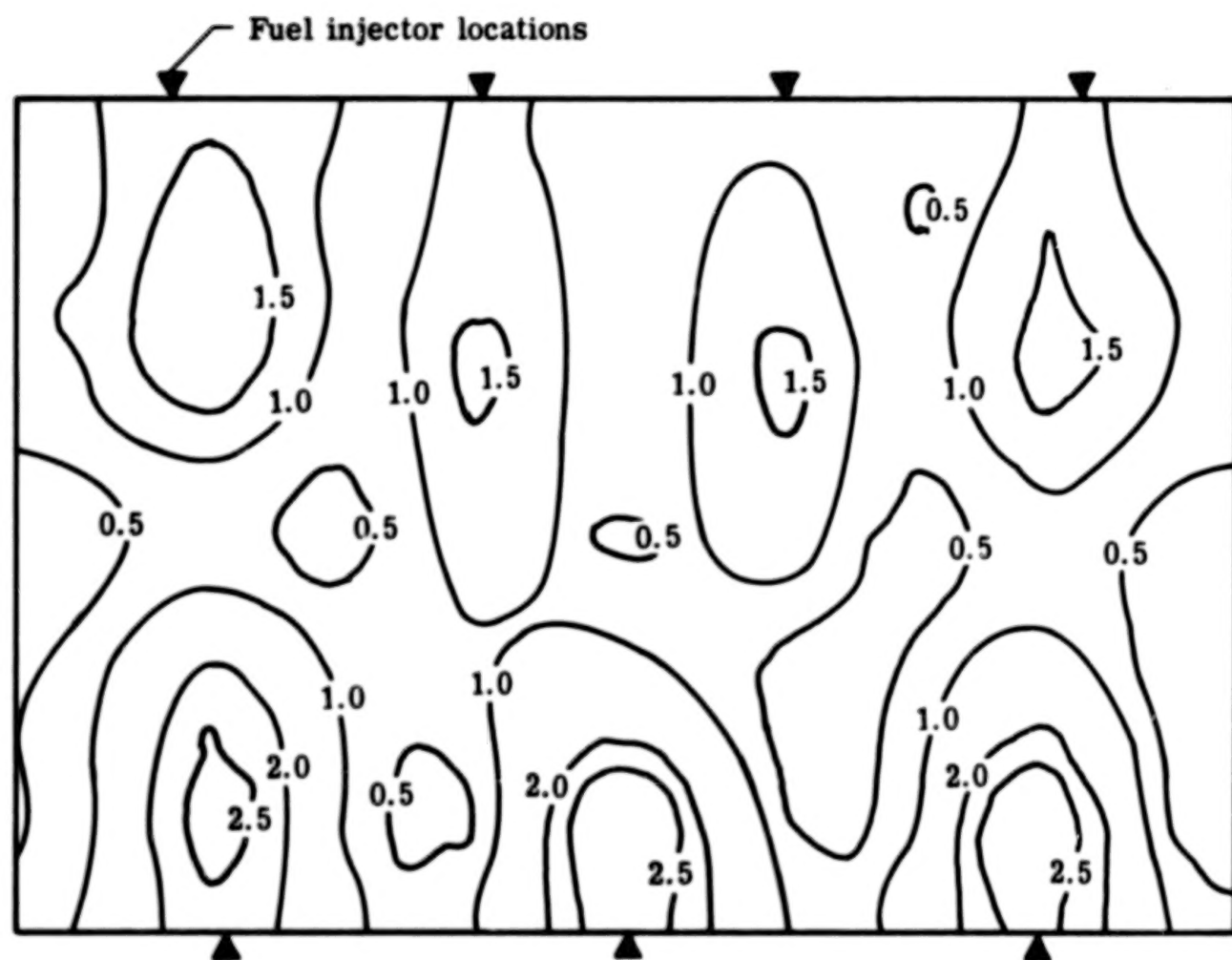
Figure 19.- Equivalence ratio contours at model exit. Configuration Q_3; $\phi = 0.87$.
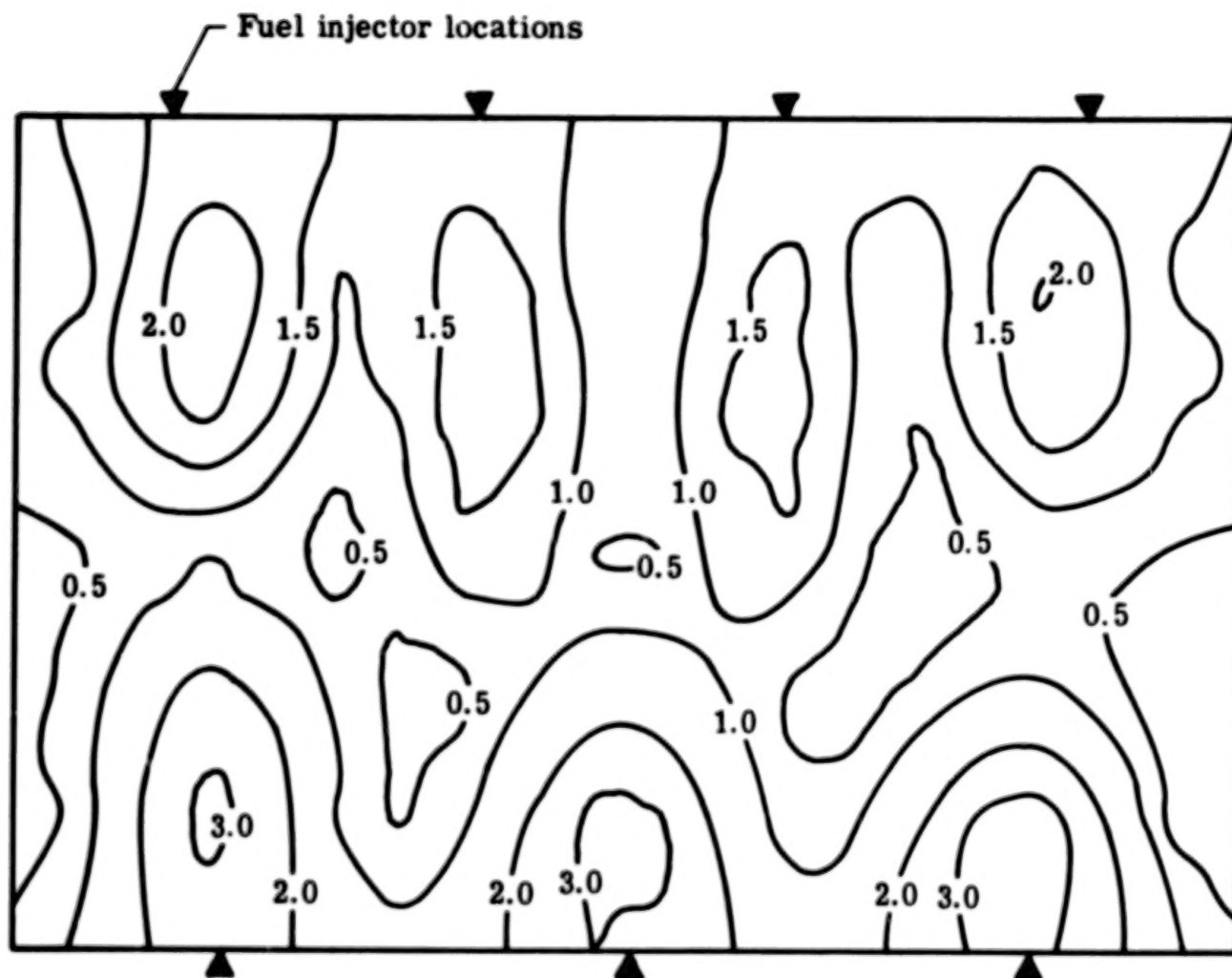
Figure 20.- Equivalence ratio contours at model exit. Configuration Q_1; $\phi = 0.92$.
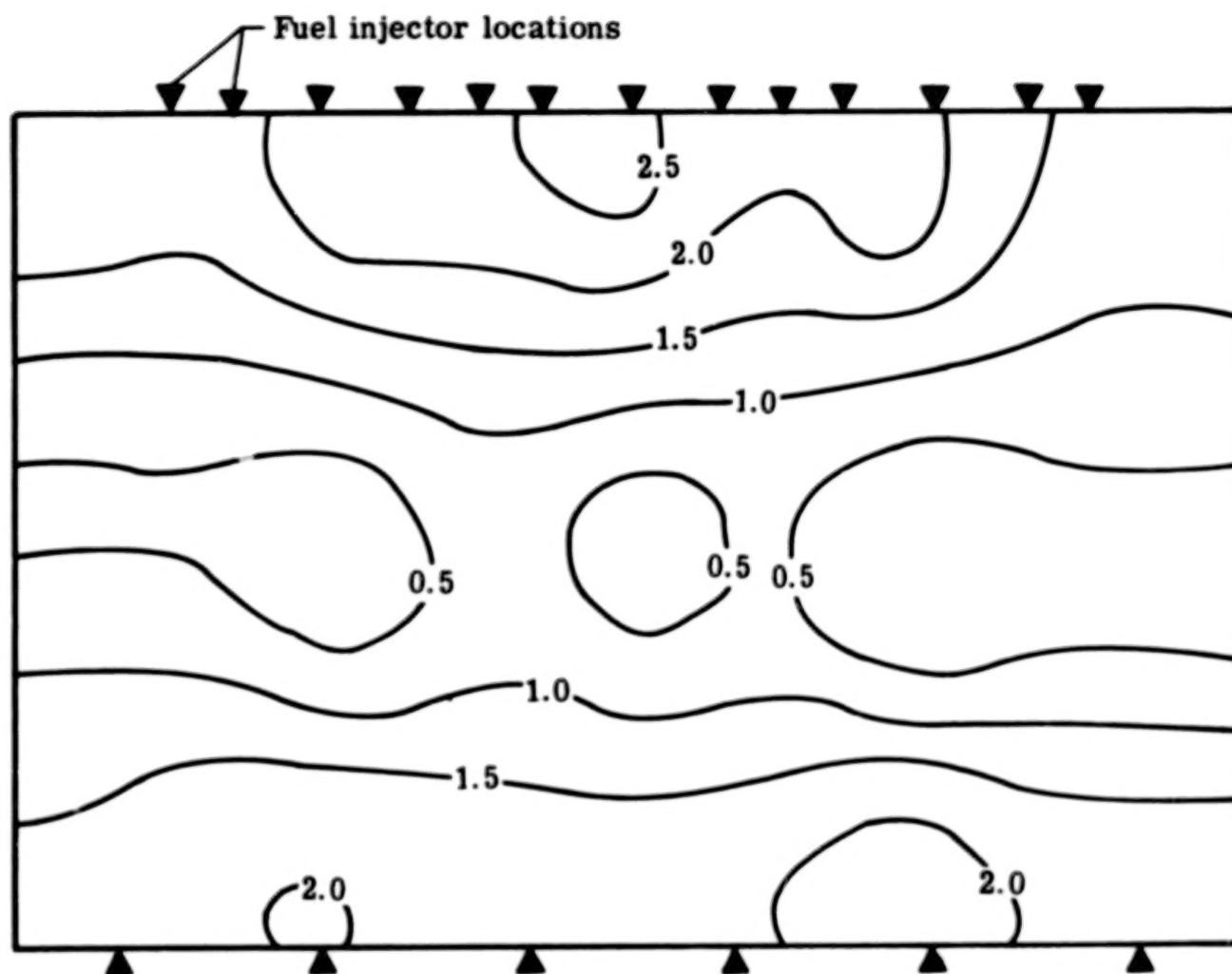
Figure 21.- Equivalence ratio contours at model exit. Configuration A$_X$; ϕ = 0.90.
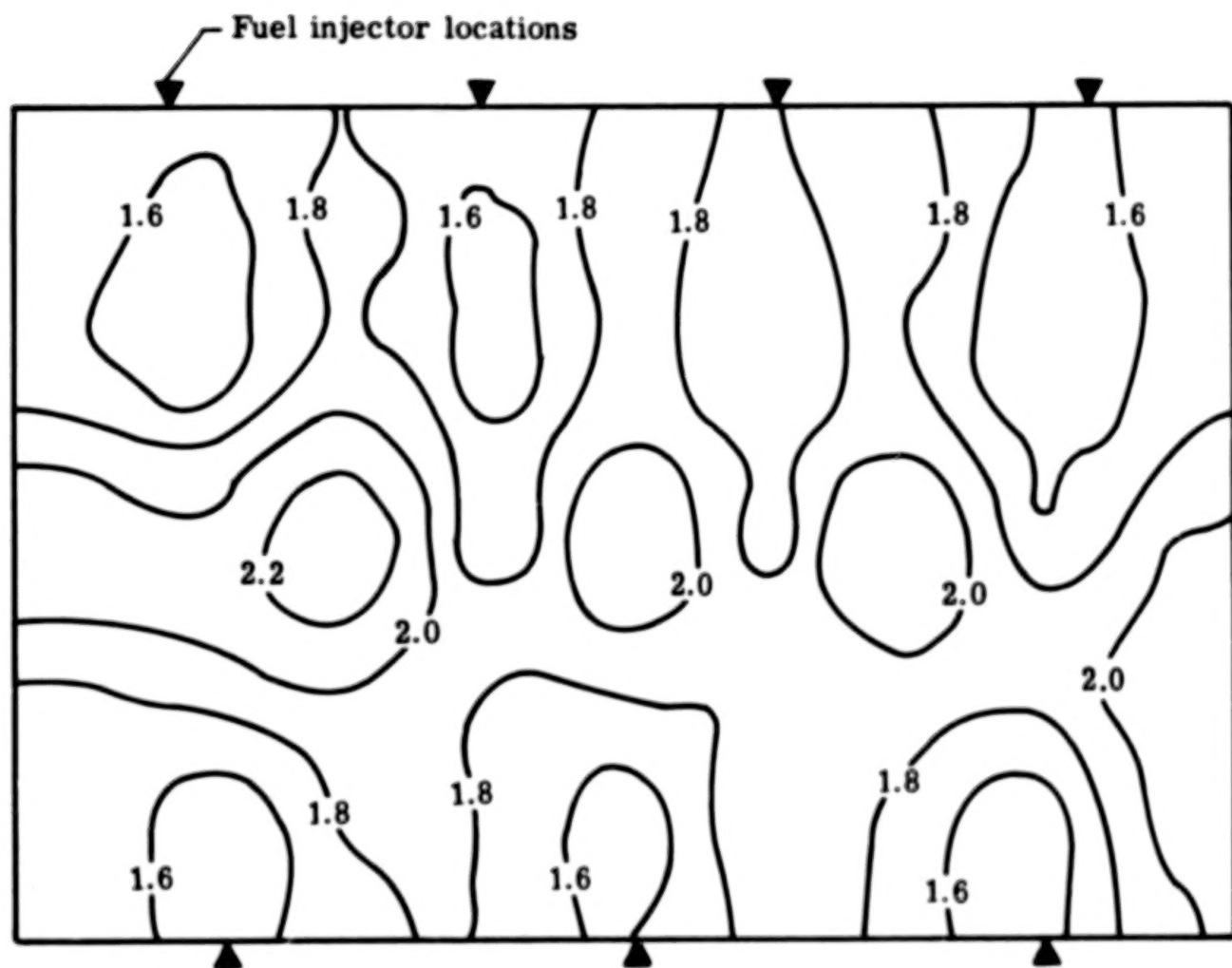
Figure 22.- Mach number contours at model exit. Configuration Q$_3$; ϕ = 0.87.

Fuel injector locations
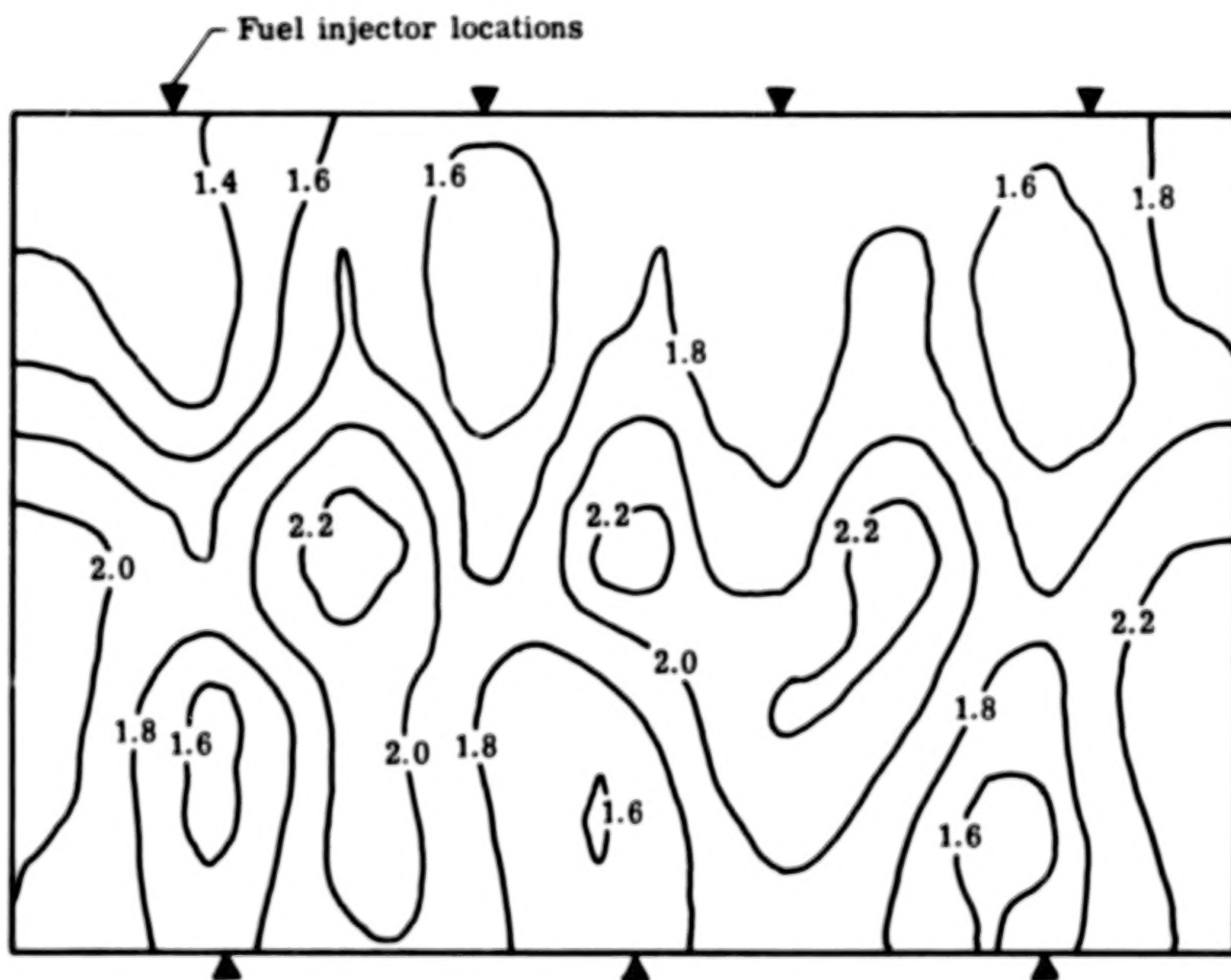
Figure 23.- Mach number concours at model exit. Configuration Q_1; $\phi = 0.92$.
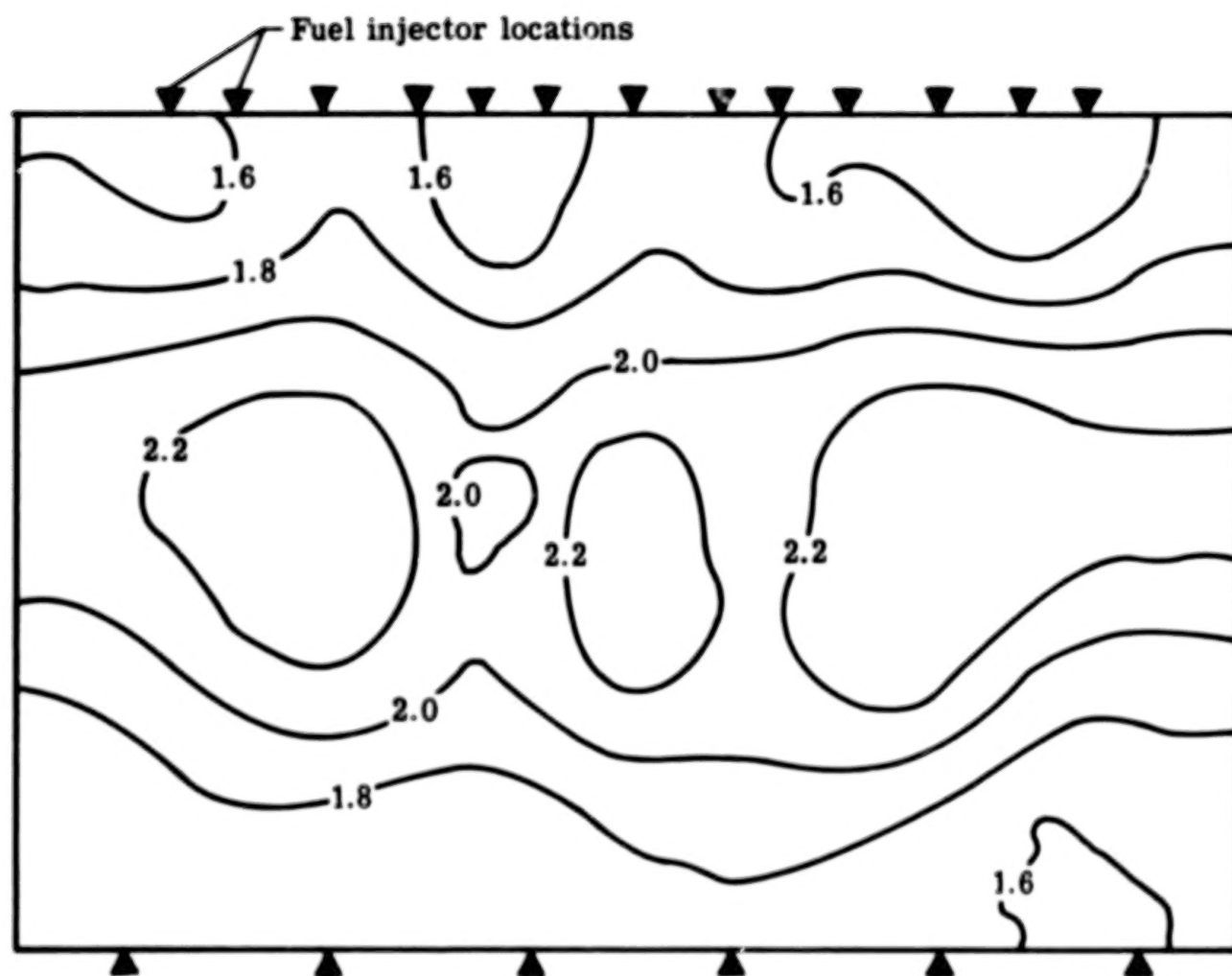
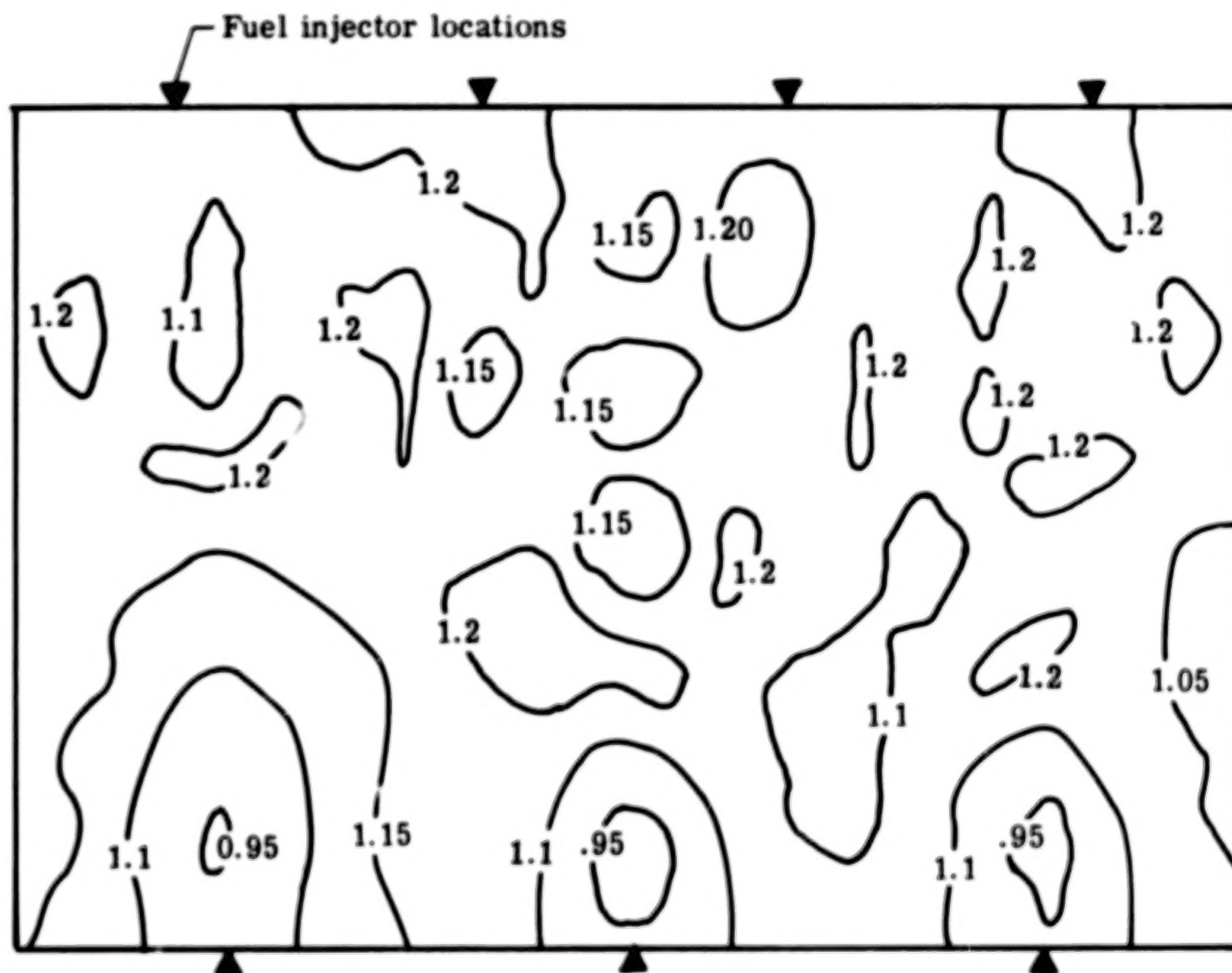Figure 24.- Mach number contours at model exit. Configuration A_X; $\phi = 0.90$.

Figure 25.- Contours of total temperature divided by combustion heater total temperature. Configuration Q_3; $\phi = 0.87$.
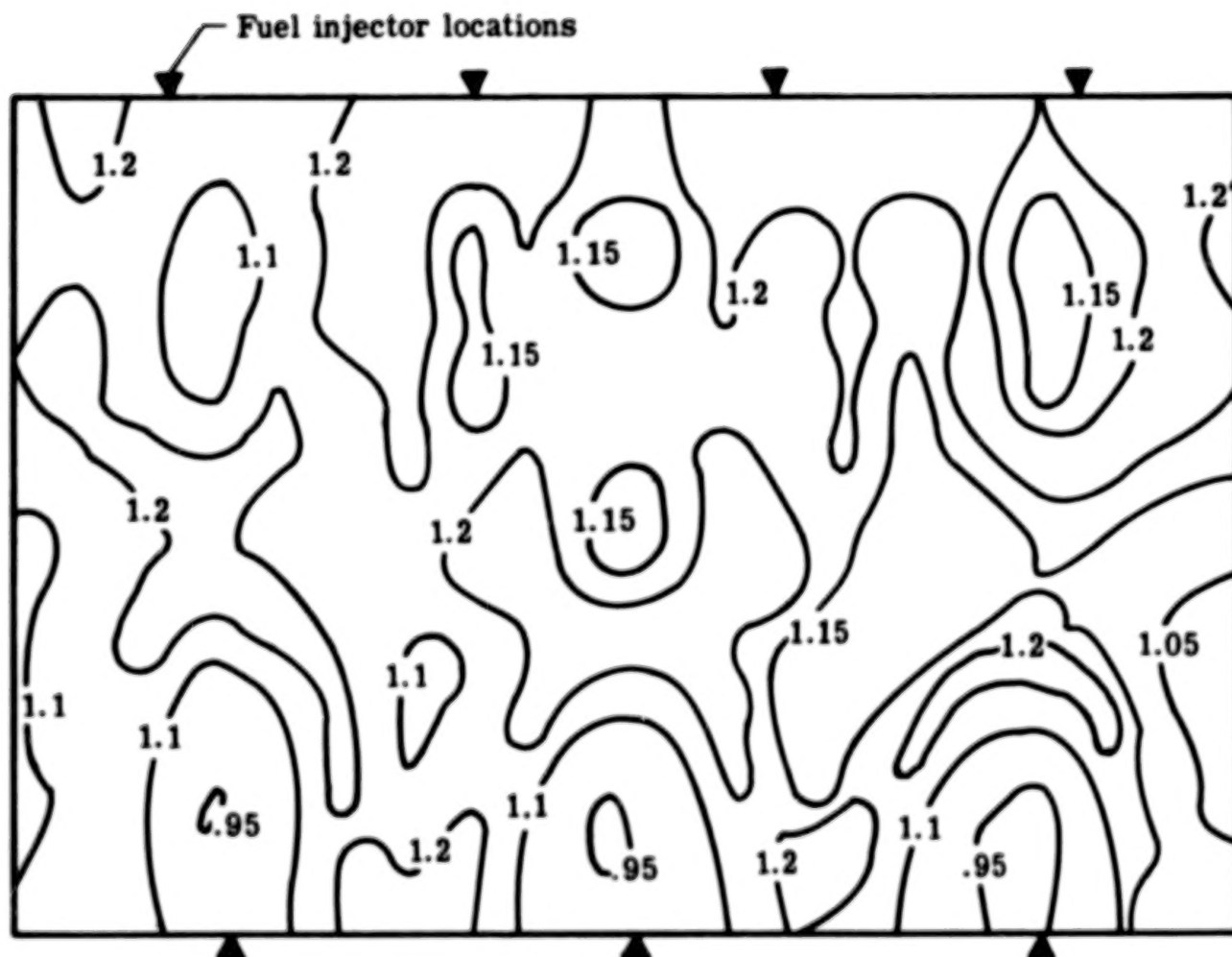
Figure 26.- Contours of total temperature divided by combustion heater total temperature. Configuration Q_1; $\phi = 0.92$.
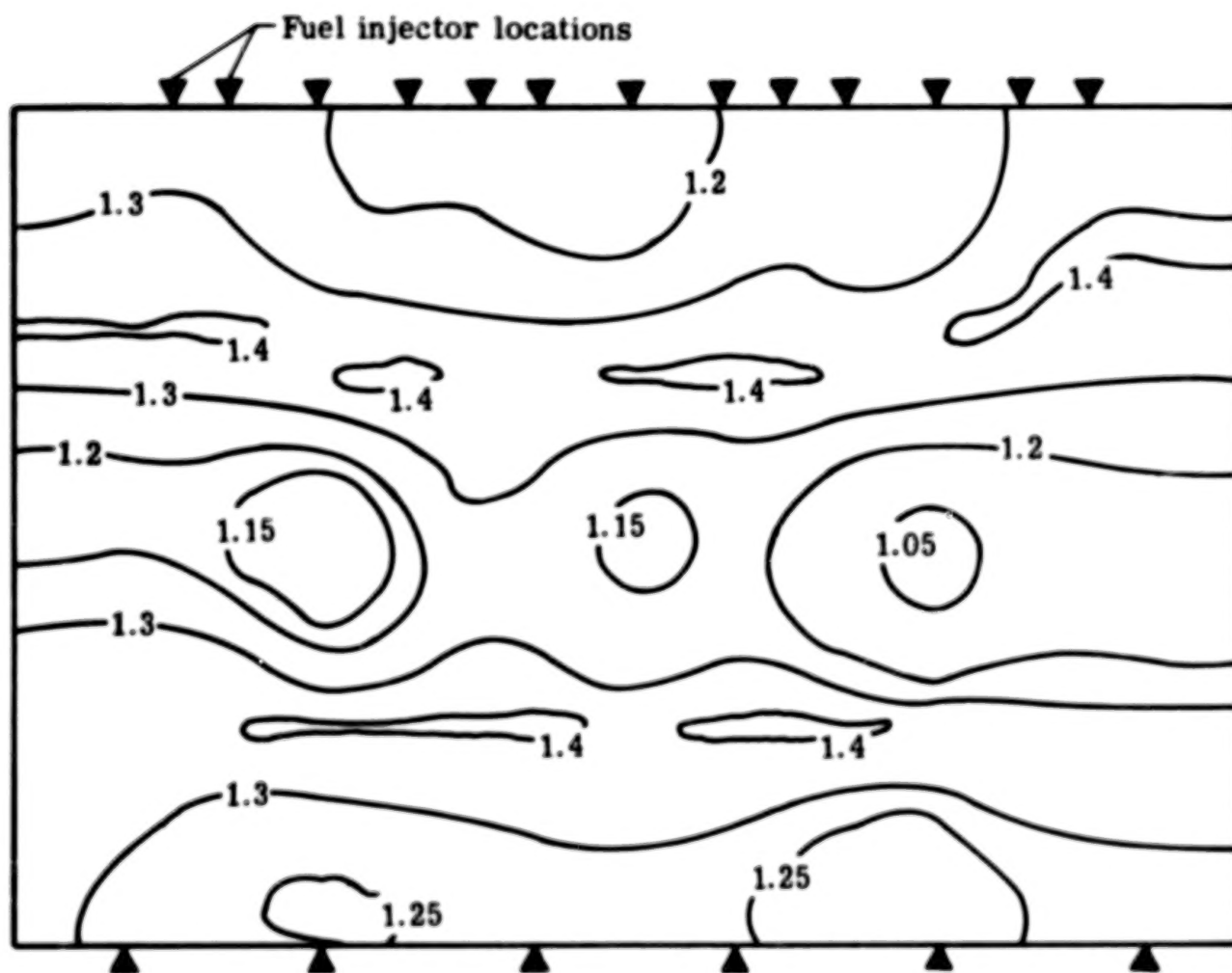
50

Figure 27.- Contours of total temperature divided by combustion heater total temperature. Configuration A_X; $\phi = 0.90$.
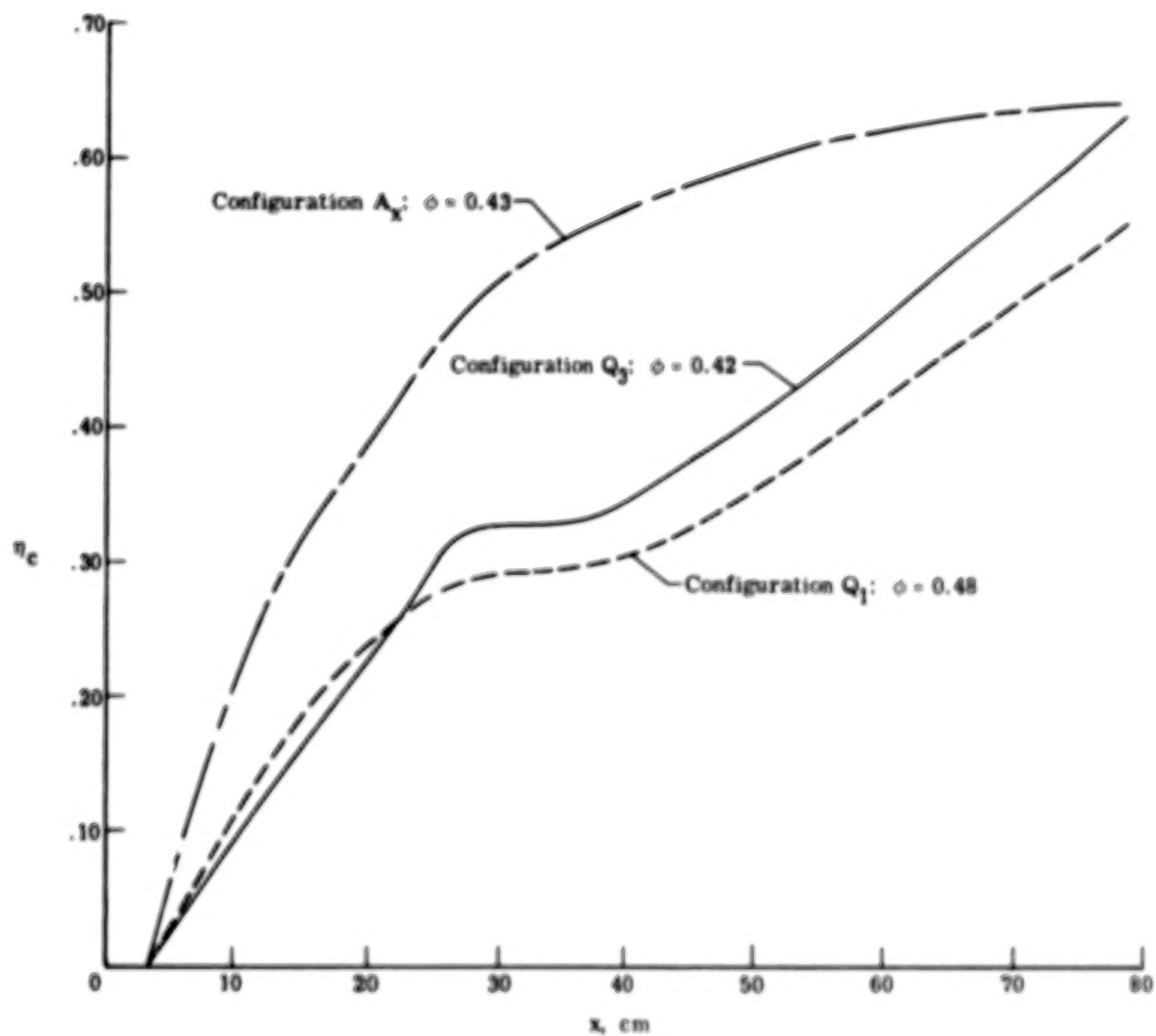
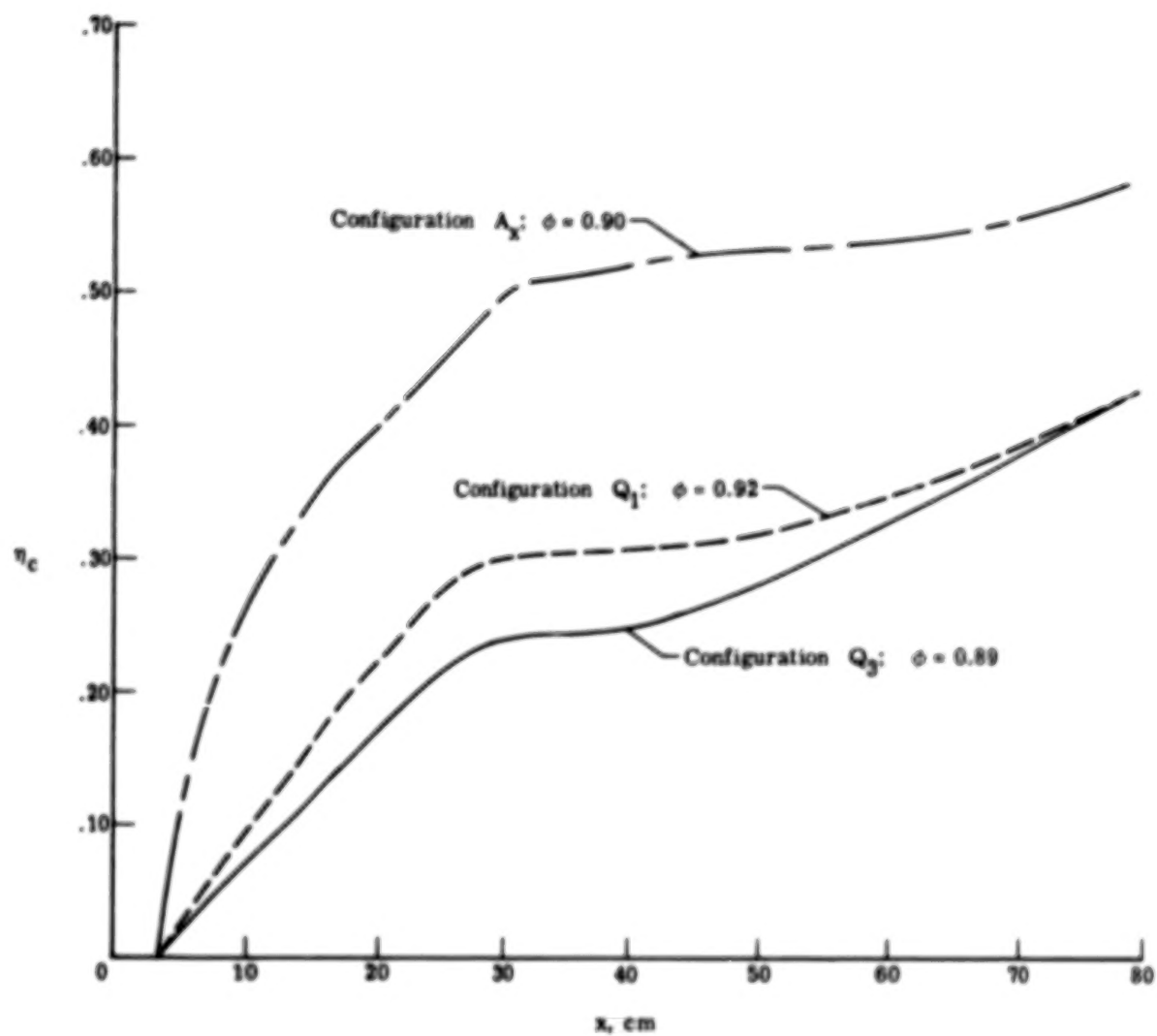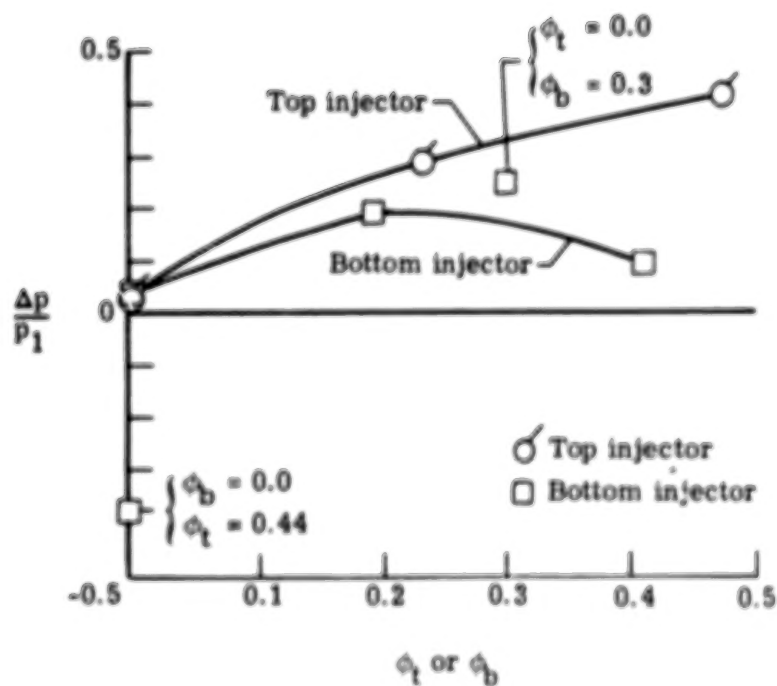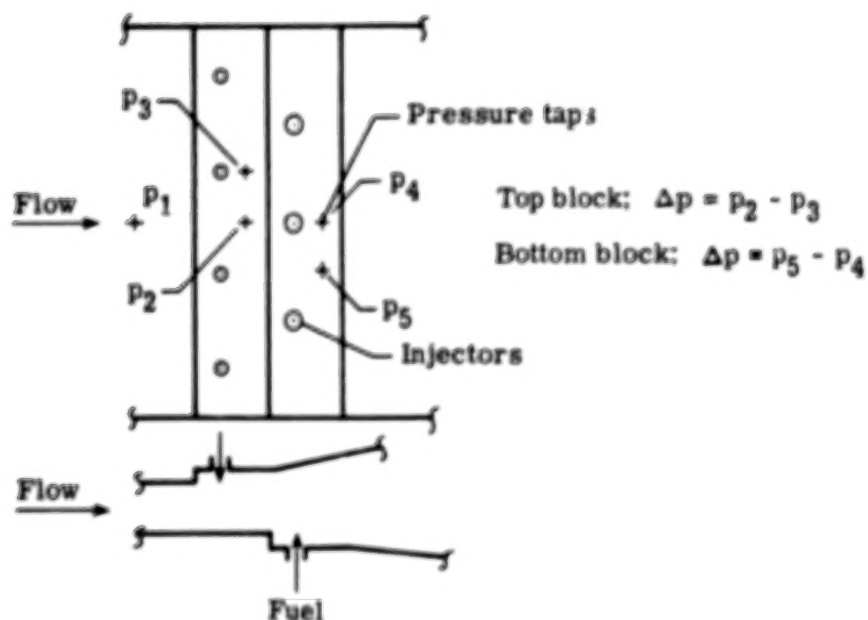Figure 28.- Combustion efficiency distribution for nominal $\phi = 0.5$ tests.

52

Figure 29.- Combustion efficiency distribution for nominal $\phi = 1.0$ tests.

Flow →

P_3

P_1

P_2

Pressure taps

P_4

P_5

Injectors

Top block; $\Delta p = p_2 - p_3$

Bottom block; $\Delta p = p_5 - p_4$

Flow →

Fuel

$\begin{cases} \phi_t = 0.0 \\ \phi_b = 0.3 \end{cases}$

Top injector

Bottom injector

Fuel schedule

ϕ_t	ϕ_b
0.0	0.0
.23	.19
.44	.0
.47	.41
.0	.30*

*Poorer quality data point

♂ Top injector

□ Bottom injector

$\frac{\Delta p}{p_1}$

$\begin{cases} \phi_b = 0.0 \\ \phi_t = 0.44 \end{cases}$

-0.5   0.1   0.2   0.3   0.4   0.5

0.5

0

ϕ_t or ϕ_b

Figure 22. - Dual-injector block pressures as a function of equivalence ratio.

1. Report No. NASA TP-1159	2. Government Accession No.	3. Recipient's Catalog No.
4. Title and Subtitle COMBUSTION OF HYDROGEN IN A TWO-DIMENSIONAL DUCT WITH STEP FUEL INJECTORS		5. Report Date May 1978
		6. Performing Organization Code
7. Author(s) James M. Eggers, Patricia G. Reagon, and Paul B. Gooderum		8. Performing Organization Report No. L-11981
9. Performing Organization Name and Address NASA Langley Research Center Hampton, VA 23665		10. Work Unit No. 505-05-41-07
		11. Contract or Grant No.
12. Sponsoring Agency Name and Address National Aeronautics and Space Administration Washington, DC 20546		13. Type of Report and Period Covered Technical Paper
		14. Sponsoring Agency Code

15. Supplementary Notes

16. Abstract

An investigation of the combustion of hydrogen perpendicularly injected from step fuel injectors into a Mach 2.72, 2100 K vitiated test gas was conducted. The model simulated the flow between the center and side struts of an integrated scramjet module at Mach 7 flight and an altitude of 29 km. Parametric variation included equivalence ratio, fuel dynamic pressure ratio, and area distribution of the model. The overall area ratio of the model was held constant at 2.87. The data analysis indicated that no measurable improvement in mixing or combustion efficiency was obtained by varying the fuel dynamic pressure ratio from 0.79 to 2.45. Computations indicated approximately 80 percent of the fuel was mixed so that it could react; however, only approximately 50 percent of the mixed fuel actually reacted in two test configurations, and 74 percent in later tests where less area expansion of the flow occurred. This poor reaction is believed to be associated with adverse pressure interactions of the upstream injection process upon the downstream injection region. One-dimensional analysis also suggests that flow expansion tended to suppress the rate of reaction. The inability of the sample probe to quench the reaction in the gas samples prevented determination of local combustion efficiencies. Recommendations for future work are also discussed.

17. Key Words (Suggested by Author(s)) Combustion Scramjet	18. Distribution Statement Unclassified - Unlimited
	Subject Category 07

19. Security Classif. (of this report) Unclassified	20. Security Classif. (of this page) Unclassified	21. No. of Pages 54	22. Price* $5.25